2.4 APPLICATION OF FRACTURE MECHANICS TECHNOLOGY.

2.4.1 Selection of Materials.

In the material selection and design of a tension-loaded structure, such as a pressure vessel, the following questions must be considered:

1. What are the critical flaw sizes (sizes which cause failure) in the different parts of the structure at expected operational stress levels?

2. What are the maximum initial flaw sizes likely to exist in the structure before service?

3. Will these initial flaws grow to critical size and cause failure during the expected service life of the structure?

The answers to these questions depend heavily upon the inherent fracture toughness and subcritical flaw-growth characteristics of the structural material. Fracture toughness data derived from test specimens are used in fracture mechanics analysis to predict critical flaw sizes, evaluate subcritical flaw growth, and estimate structural life. They can also be used to determine the maximum possible initial flaw size in a structure after a proof load.

As previously mentioned (Section 2.2), the types of flaws encountered in fabricated structures can be categorized as surface flaws, embedded flaws, and through-the-thickness cracks. For surface and embedded flaws, the degree of constraint at the crack leading edge is high, and plane-strain conditions generally prevail. The initial flaws may or may not reach critical size before growing through the thickness, depending upon the plane-strain fracture toughness (K_{Ic}) value, the applied stress levels, and the material thickness. If the calculated critical flaw size is small with respect to the wall thickness, the formation of a through-the-thickness crack before fracture is not likely.

For through-the-thickness cracks, the mode of fracture for a given material, stress level, and test temperature depends upon the material thickness. If the material is relatively thin, plane-stress conditions generally predominate. With increasing thickness, the fracture appearance changes from that of full shear to an essentially flat or plane-strain fracture. Thus, for thin sections containing through-the-thickness cracks, the plane-stress fracture thoughness (K_c) values are important, and as the thickness is increased the plane-strain (K_{Ic}) values should be used. The theory of this has been discussed in detail (Section 2.2.2).

The common types of fracture specimens and their requirements have also been discussed (Section 2.2.3). It is appropriate to point out the significance of end-hardware application and material anisotropy on specimen selection and to show fracture-toughness correlations among several of the more common specimens.

Just as conventional mechanical properties generally vary to some degree among various forms and grain directions in a given basic alloy, it has been found from fracture tests performed thus far on various materials that fracture toughness values also vary. In a rolled plate or forging, six directions of flaw propagation are possible, and plane-strain toughness (K_{Ic}) values may differ in each of these directions (Fig. E2-17). The need to determine the K_{Ic} values in each of these directions depends on the direction of the applied stresses in the hardware.

Considering the banding and delamination problems in some thick plates, it appears that the K_{Ic} values can be different between the A and B directions and, likewise, the C and D directions. This has actually been found to be the case from investigation (Ref. 16) and tends to explain the differences in K_{Ic} values obtained using surface-flawed and round-notched-bar or single-edge-notched fracture specimens. The surface-flawed specimen

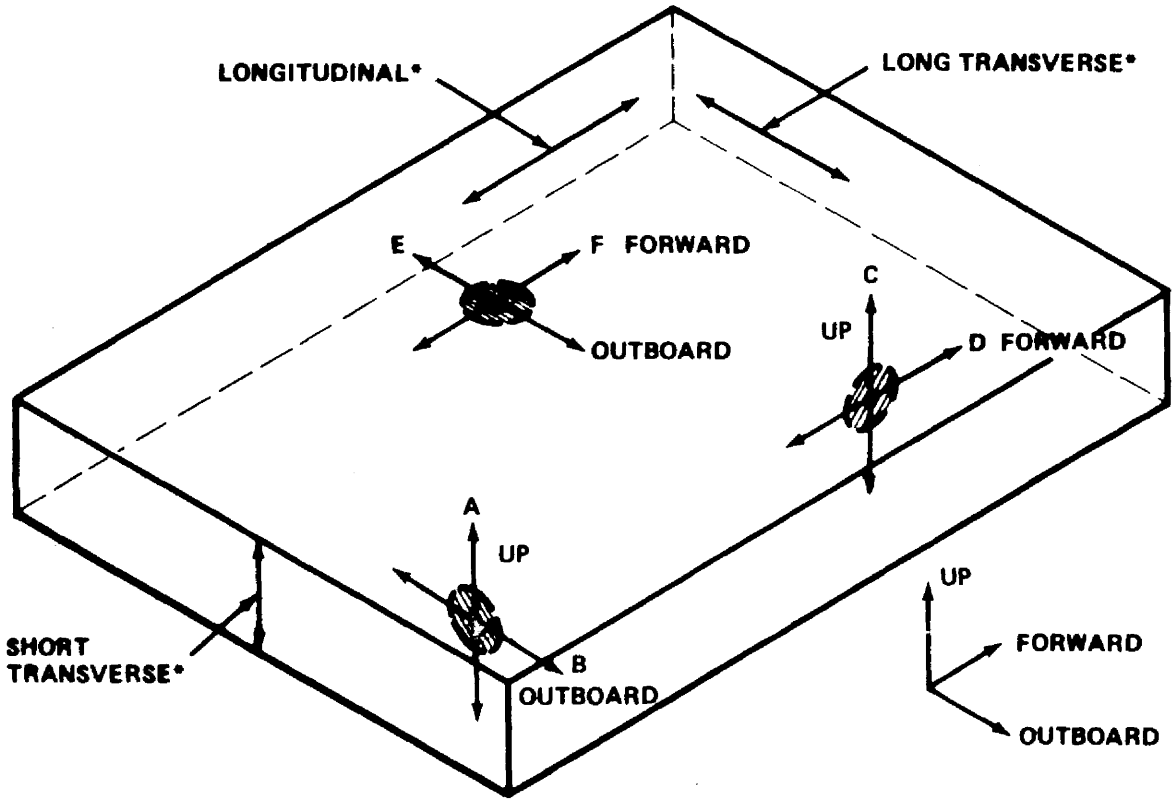

FIGURE E2-17. STRESS FIELD, GRAIN DIRECTIONS, AND POSSIBLE DIRECTIONS OF FLAW PROPAGATION

is normally used to measure toughness in either the A or C directions, and the single-edge-notched or center-cracked (pop-in) specimens measure toughness in the B or D directions. The round notched bar (removed so that its longitudinal axis is parallel to the plate surface) measures the lower of either the A or B directions or the lower of either the C or D directions. For material where there are no pronounced directional effects, the same toughness should be obtained regardless of which specimen is used. In the short transverse direction of materials, there appears to be no reason for a significant difference in K_{Ic} values between the E and F directions, although there is no apparent experimental substantiation of this.

For weldments, it is known that there can be differences in fracture toughness between the weld centerline and the heat-affected zone. In addition, it is considered probable that fracture toughness as well as subcritical flaw growth characteristics vary within the heat-affected zone so that for the establishment of realistic allowable flaw sizes, the minimum K_{Ic} values must be determined.

The foregoing discussion makes clear the necessity for insuring the use of comparable valid fracture toughness and subcritical flaw growth data when they are available, or the selection of proper specimen types to obtain the desired directional data, in comparing materials for selection. While round-notched-bar specimens might be considered desirable because they automatically obtain the lower toughness values in either the A or B directions or the lower in either the C or D directions, it may not always be possible to use the specimen type because of material thickness limitations (i.e., the required specimen diameter for valid K_{Ic} exceeds the hardware wall thickness). In such a case, the single-edge-notched specimen might be used for toughness in the B and D directions and the surface-flawed specimen in the A and C directions.

In summary, it presently appears that there is no single "best fracture specimen" to use in all situations where toughness data are needed for material comparisons and selection, nor is such required. Of primary importance is that the selected specimen toughness data for different materials provide a valid comparison for selection and be representative of toughness and flaw growth characteristics of the material as used in the hardware application.

2.4.1.1 Static Loading.

An evaluation of the resistance of materials to catastrophic brittle fracture requires the following basic material properties:

1. Plane-strain fracture toughness, K_{Ic}.

2. Conventional tensile yield strength, σ_{ys}.

An evaluation of materials based on the data accumulated from test specimens can be illustrated best by using a hypothetical example.

I. Example Problem A.

Three materials — a steel, a titanium, and an aluminum alloy — are initially selected as potential candidate materials for minimum weight design. The yield strength of each is chosen to attain nearly equivalent strength/weight ratios. The yield strengths and K_{Ic} values obtained from the tested specimens and design requirement are shown in the following table.

Alloy	Density (lb/in.^{3})	σ_{ys} (ksi)	σ_{ys}/Density $\times$ 1000 (in.)	K_{Ic}, (ksi $\sqrt{\text{in.}}$)	Applied Stress 1/2 σ_{ys} (ksi)
Steel	0.284	250	880	100	125
Aluminum	0.098	85	870	30	42.5
Titanium	0.163	140	860	80	70

Assume that

1. The defect is a semielliptical surface flaw with $a/2c = 0.2$.

2. The defect is located in a thick plate loaded in tension.

To decide which material provides the most fracture resistance is to establish which material requires the largest critical flaw size for catastrophic fracture.

For "thick walled" structures critical flaw sizes can be determined from the following equation:

$$(a/Q)_{cr} = \frac{1}{1.21\pi}\left(\frac{K_{Ic}}{\sigma}\right)^2$$

or

$$a_{cr} = \frac{Q}{1.21\pi}\left(\frac{K_{Ic}}{\sigma}\right)^2$$

where the shape factor parameter can be obtained from Fig. E2-5. For this comparison, $Q = 1.26$.

The results are shown in the following table.

Alloy	Depth, a_{cr} (in.)	Length, 2c (in.)
Steel	0.212	1.06
Aluminum	0.165	0.83
Titanium	0.432	2.16

Conclusion.

The titanium alloy is most fracture resistant in terms of requiring the largest critical flaw size defect, a_{cr}, for catastrophic fracture.

This conclusion could have been reached by considering the K_{Ic}/σ_{ys} ratios for the various materials shown in the following table.

Alloy	K_{Ic}/σ_{ys} ($\sqrt{\text{in.}}$)
Steel	0.400
Aluminum	0.353
Titanium	0.572

The titanium, having the highest K_{Ic}/σ_{ys} ratio, could be expected to be the toughest material for the given application.

Tiffany and Masters (Ref. 17) showed that for screening several materials, K_{Ic} data are often plotted as shown in Fig. E2-18a. Recognizing that the operating stress levels are generally controlled to a fixed percentage of the unflawed tensile strength by the design safety factor, the data shown in Fig. E2-18a might be more appropriately plotted as shown in Fig. E2-18b. The ordinate is directly proportional to the critical flaw size, thus placing the influence of varying materials strength in better perspective. From Fig. E2-18b the three materials can be compared upon the basis of equal critical flaw size. For example, structures designed from a 200-ksi steel, a 135-ksi titanium, and a 70-ksi aluminum would all have approximately the same critical flaw size. Considering the effect of weight, one might wish to make the comparison shown in Fig. E2-18c. This shows that titanium provides a somewhat lighter tank on the basis of equal flaw size.

Based on considerations of the practical capability of available nondestructive inspection (NDI) techniques, the resistance to catastrophic fracture could also be evaluated by calculating the maximum allowable applied stress for equivalent defects in each material.

Reevaluate the preceding example, assuming that the minimum detectable flaw is 0.15 in. deep by 0.75 in. long.

Rearranging the basic equation results in

$$\sigma^2 = \frac{K_{Ic}^{\ 2}\,(Q)}{1.21\pi\,(a)} \quad .$$

The resulting critical fracture stresses and other pertinent information are summarized in the following table.

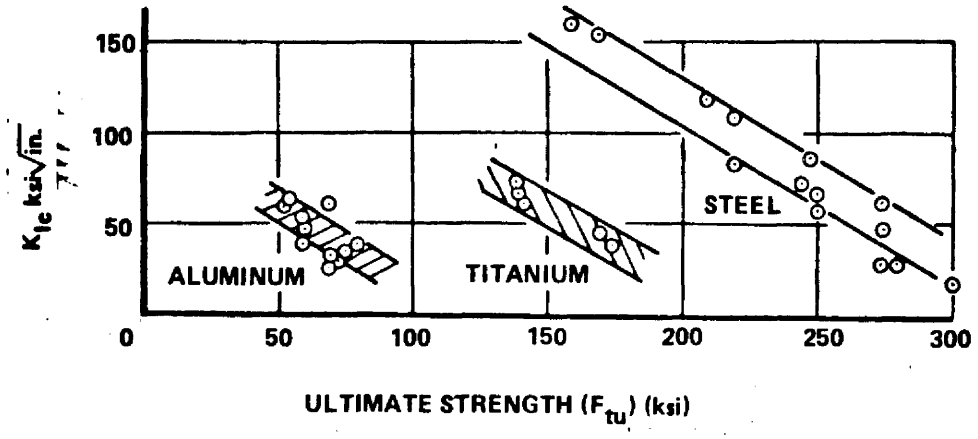

a.

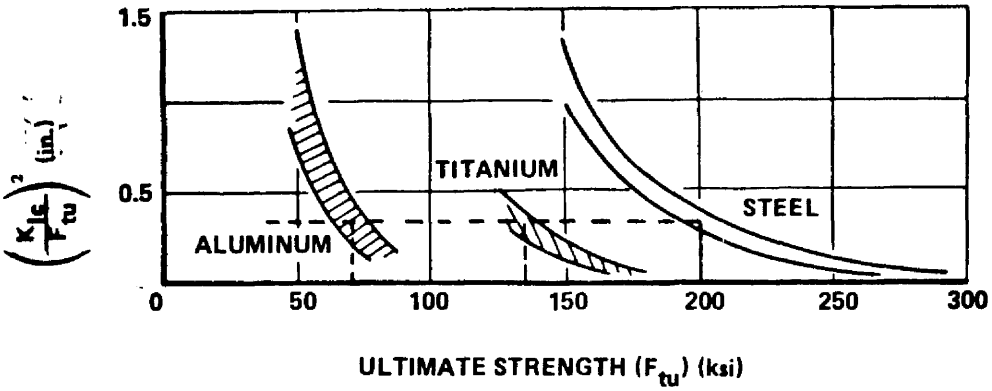

b.

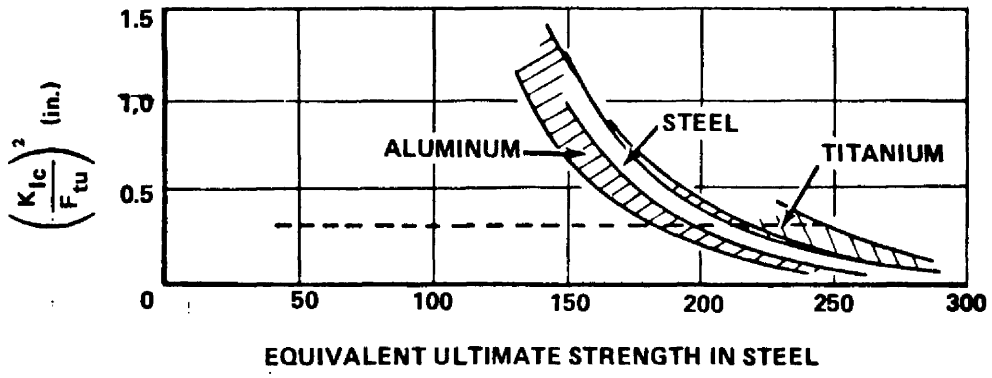

c.

FIGURE E2-18. MATERIAL COMPARISONS (BASE METAL, ROOM-TEMPERATURE TRENDS)

Alloy	σ_{ys} (ksi)	Design Stress $0.5\,\sigma_{ys}$ (ksi)	Fracture Stress σ (ksi)	Safety Factor $\sigma/0.5\,\sigma_{ys}$
Steel	250	125	144	1.15
Aluminum	85	42.5	43	1.01
Titanium	140	70	112	1.60

From the above data it is apparent that the titanium provided the greatest safety factor and resistance to fracture.

2.4.1.2 Cyclic or Sustained Loading.

An evaluation of the resistance of materials to fracture requires the consideration of the crack growth rate characteristics in addition to other material properties.

Some examples of data obtained from tests are shown in Figs. E2-19 and E2-20 (Ref. 18). The realistic and practical approach for comparing materials is to evaluate their crack growth characteristics under a given application condition. Let us consider the following hypothetical example.

I. Example Problem A.

1. Materials to be considered are the steel and aluminum alloys for which the data are given in Figs. E2-19 and E2-20.

2. The component of interest is a thick plate cyclic loaded in tension under stresses that vary from zero to maximum tension during each cycle.

3. The design fixes σ_{max} as one-half the yield strength for each material: 88 ksi for steel and 32 ksi for aluminum.

4. The worst possible type of flaw that is envisioned is a semi-elliptical surface flaw with $a/2c = 0.20$.

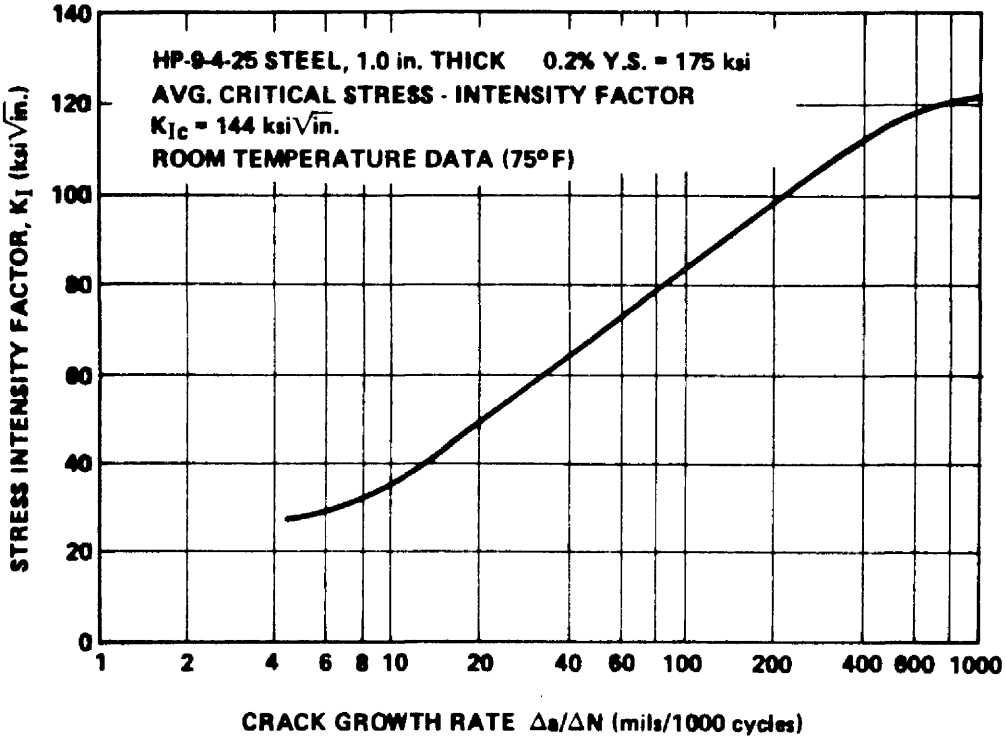

FIGURE E2-19. CRACK GROWTH RATE FOR HP-9-4-25 STEEL

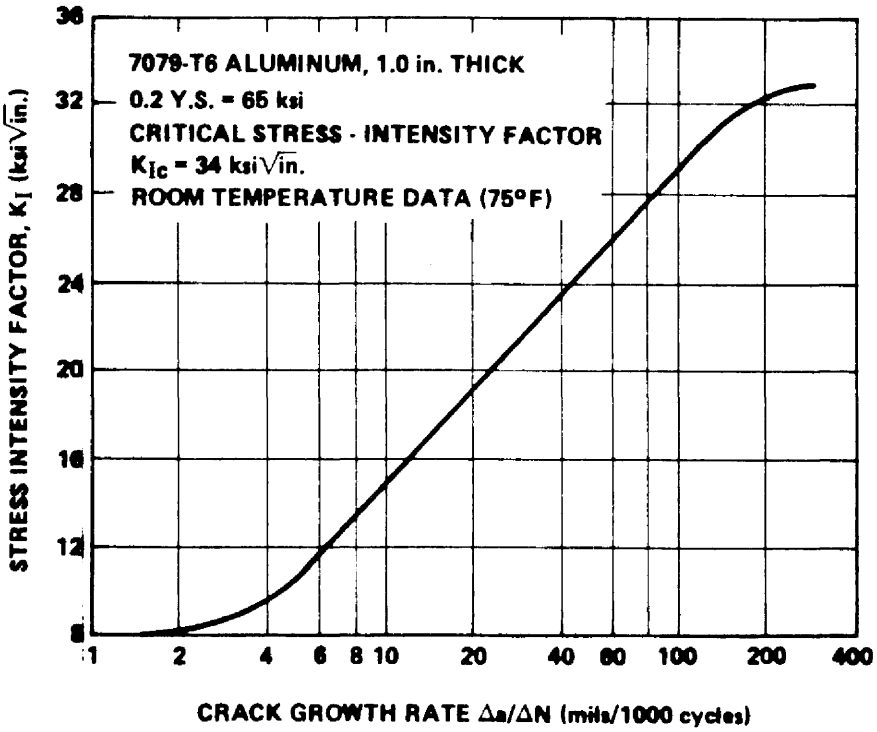

FIGURE E2-20. CRACK GROWTH RATE FOR 7079-T6 ALUMINUM

5. The minimum size flaw that could be detected by the NDI technique is 0.15 in. deep by 0.72 in. long. Therefore, each material is assumed to contain this flaw.

Under these circumstances, which material has the longest life?

Solution.

Step 1. The first step is to compute the value of the initial stress intensity, K_{Ii}, for each material for the prevailing conditions of defect size and stress. The appropriate expression for K_{Ii} for the stipulated defect and component geometry is

$$K_{Ii}^2 = \frac{1.21 \pi a \sigma^2}{Q}$$

where

a = crack = 0.15 in. = specified,

σ = applied stress (maximum during cycle) = 1/2 σ_{ys} each materia',

steel = 88 ksi, aluminum = 32 ksi,

σ_{ys} = yield strength, steel = 175 ksi, aluminum = 65 ksi,

and

Q = 1.26 for specified flaw geometry.

The calculations reveal the following:

$$K_{Ii}^2 = \frac{1.21 \pi (0.15) (88\ 000)^2}{1.26}$$

and

$$K_{Ii} = 59\,000 \text{ psi} \sqrt{\text{in.}}$$

for steel, and

$$K_{Ii}^2 = \frac{1.21\,\pi\,(0.15)\,(32\,000)^2}{1.26}$$

and

$$K_{Ii} = 21\,500 \text{ psi} \sqrt{\text{in.}}$$

for aluminum.

The crack growth rates for the two materials at the beginning of life can now be determined from Figs. E2-19 and E2-20 using their respective K_I values for the imposed conditions. The results are shown in the following table.

Alloy	K_I (psi $\sqrt{\text{in.}}$)	Crack Growth Rates (mils/cycle)
Steel	59 000	0.035
Aluminum	21 500	0.030

However, a knowledge of the crack growth rates at the beginning of life is not sufficient to determine the respective life expectancy of each material. One must consider the change in K_I and the associated change in crack growth rates for each material as the crack grows during service as well as the threshold stress intensity, K_{TH}.

Step 2. The growth rate data illustrated in the form shown in Figs. E2-21 and E2-22 (Ref. 18) provide a convenient method for evaluating the life expectancy without becoming intimately involved with changes in K_I and growth rates. Figures E2-21 and E2-22 are constructed from the same basic test data as were used to construct Figs. E2-19 and E2-20. To utilize Figs. E2-21 and E2-22 it is necessary to know the ratio of K_{Ii} to K_{Ic}. The previous calculations in Step 1 showed that K_I is 59 ksi $\sqrt{\text{in.}}$ for steel and 21.5 ksi $\sqrt{\text{in.}}$ for aluminum. Since the K_{Ic} values for each material were known from static toughness tests, the K_{Ii}/K_{Ic} ratios are readily determined:

$$\frac{K_{Ii}}{K_{Ic}} = \frac{59\ 000}{144\ 000} = 0.41$$

for steel, and

$$\frac{K_{Ii}}{K_{Ic}} = \frac{21\ 500}{34\ 000} = 0.63$$

for aluminum.

The cyclic life corresponding to these K_{Ii}/K_{Ic} values may be determined directly from Figs. E2-21 and E2-22 — steel, 1800 cycles, and aluminum, 4000 cycles, if the time at maximum stress is short during each cycle.

Thus, for this specific example where both materials contained the same given size and type of defect and both were stressed to one-half their yield strengths, the aluminum has the greatest life expectancy.

It should be emphasized that the result of this example cannot be used to generalize the relative behavior of the two materials. For other conditions of initial defect sizes and/or applied stresses, it is possible that the steel

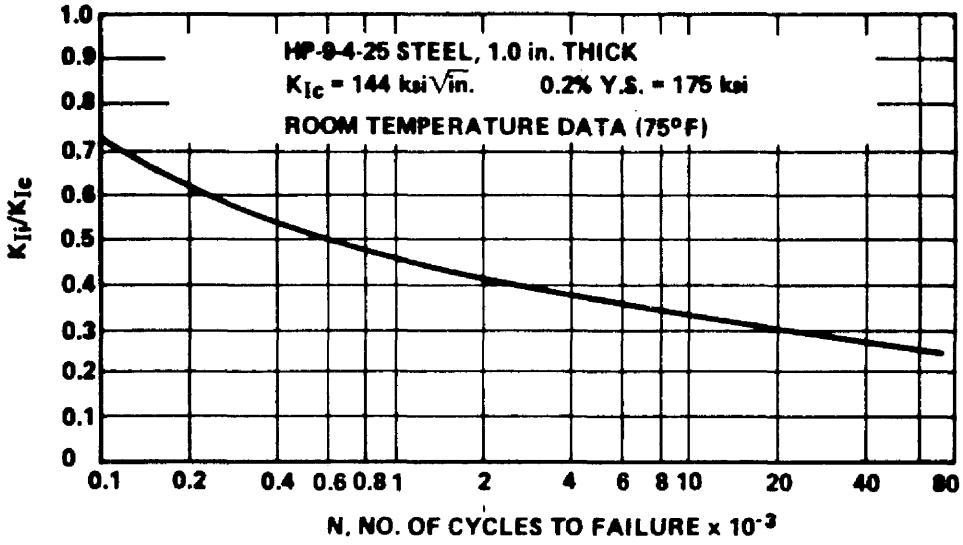

FIGURE E2-21. COMBINED CYCLIC FLAW GROWTH DATA FOR HP-9-4-25 STEEL PLATE

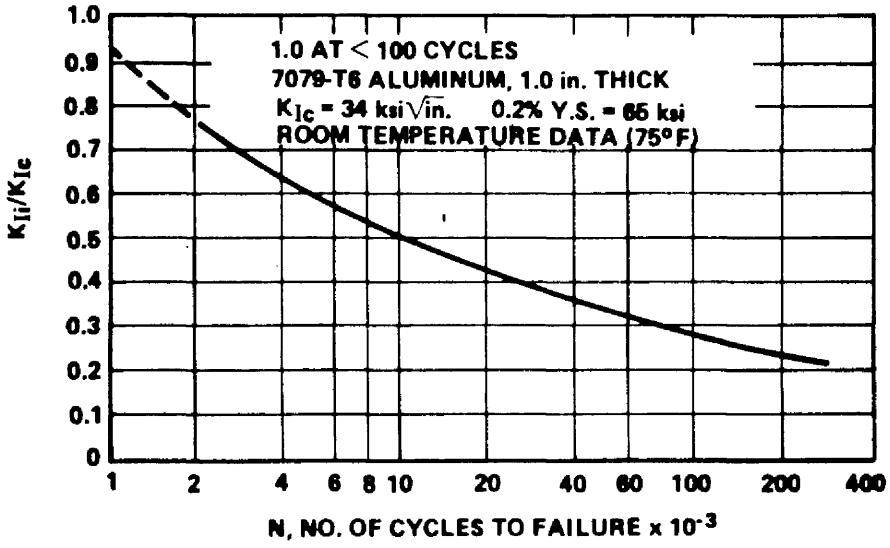

FIGURE E2-22. COMBINED CYCLIC FLAW GROWTH DATA FOR 7079-T6 ALUMINUM PLATE

could have the greater life expectancy. This is demonstrated in the following table, which shows the life expectancy of the two materials for a wide range of initial defect sizes and for a constant applied stress of $\sigma_{ys}/2$.

Initial Defect Depth a_i (in.)	Initial Stress-Intensity Factor K_{Ii} (ksi $\sqrt{\text{in.}}$)		$\frac{K_{Ii}}{K_{Ic}}$		Cycles to Failure N (Life Expectancy)	
	Steel	Aluminum	Steel	Aluminum	Steel	Aluminum
0.05	19.6	7.2	0.136	0.210	$>>300 \times 10^3$	300×10^3
0.07	27.5	10.1	0.191	0.297	$>100 \times 10^3$	100×10^3
0.10	39.4	14.3	0.274	0.420	30×10^3	21×10^3
0.15	59.0	21.5	0.410	0.632	1.8×10^3	4×10^3
0.20	78.8	28.7	0.540	0.845	0.37×10^3	1.5×10^3
0.25	98.4	35.9	0.683	>1.0	0.25×10^3	---

From the table it is seen that when the initial defect depth is 0.15 in. or larger, the aluminum will have the longer life N. However, when the initial defect depth is 0.10 in. or smaller, the steel will have the greater life expectancy. Although the steel has the larger absolute value of fracture toughness, K_{Ic}, and therefore has the largest critical crack size for catastrophic failure, it also has a greater crack growth rate for a given change in K as seen from the differences in slope of the growth rate curves shown in Figs. E2-23 and E2-24 (Ref. 18). Therefore, it is possible to have a "crossover" situation between the life expectancies of steel and aluminum, as noted in the table.

Again, the life expectancies in preceding table reflect short time at maximum cyclic stress. If the time at maximum stress is long, the portion of time that the stress-intensity level is above the threshold stress intensities

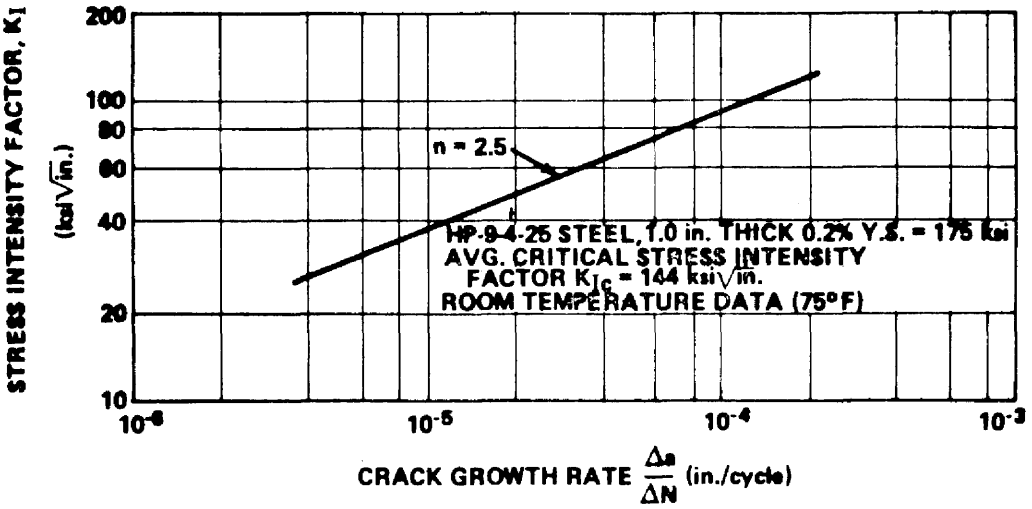

FIGURE E2-23. CRACK GROWTH RATE AS A FUNCTION OF STRESS INTENSITY FOR HP-9-4-25 STEEL

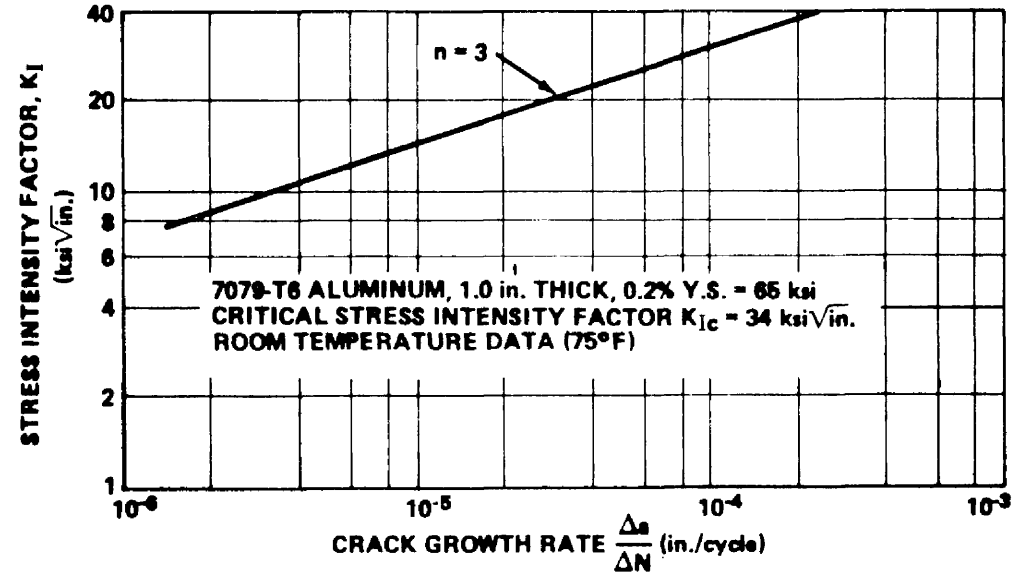

FIGURE E2-24. CRACK GROWTH RATE AS A FUNCTION OF STRESS INTENSITY FOR 7079-T6 ALUMINUM

for the steel and aluminum would cause reductions in the cyclic lives for the different initial defect sizes.

The materials could also be compared in another manner by using the data provided in Figs. E2-21 and E2-22 to answer the question of which material could tolerate the largest initial defect (of a given type) that would not grow to a critical size during some given minimum lifetime for the component.

II. Example Problem B.

Known Information:

Plate cyclic loaded (sinusoidal) in tension.

Required life — 50 000 cycles.

Applied stress (maximum stress during cycle) one-half yield strength:

steel = 88 000 psi.

aluminum = 32 000 psi.

Type of defect — semielliptical surface flaw with $a/c = 0.4$.

Fracture toughness, K_{Ic}:

steel = 144 000 psi $\sqrt{\text{in.}}$

aluminum = 34 000 psi $\sqrt{\text{in.}}$

Unknown Information: Which material can tolerate the largest initial defect?

Solution.

Step 1. From Figs. E2-21 and E2-22, find the K_{Ii}/K_{Ic} ratio corresponding to the desired life of 50 000 cycles:

$$\frac{K_{Ii}}{K_{Ic}} \text{ at 50 000 cycles} = 0.25$$

for steel, and

$$\frac{K_{Ii}}{K_{Ic}} \text{ at } 50\,000 \text{ cycles} = 0.34$$

for aluminum.

Step 2. Knowing the K_{Ic} and K_{Ii}/K_{Ic} ratio corresponding to 50 000 cycles, solve for K_{Ii}:

$$K_{Ii} = 0.25\ K_{Ic} = 0.25\ (144\,000 \text{ psi} \sqrt{\text{in.}}) = 36\,000 \text{ psi} \sqrt{\text{in.}}$$

for steel, and

$$K_{Ii} = 0.34\ K_{Ic} = 0.34\ (34\,000 \text{ psi} \sqrt{\text{in.}}) = 11\,500 \text{ psi} \sqrt{\text{in.}}$$

for aluminum.

Step 3. Since K_{Ii} depends upon stress and defect size, it is now possible to solve for defect size knowing stress. For semielliptical surface defects with $a/c = 0.4$, the following expression is appropriate:

$$a_i = \frac{K_{Ii}^2\ (Q)}{1.21\ \pi\ \sigma^2} \quad ;$$

for steel,

$$a_i = \frac{(36\,000)^2\ (1.26)}{1.21\ \pi\ (88\,000)^2}$$

and

$$a_i = 0.056 \text{ in.}$$

when the defect is 0.056 in. deep by 0.28 in. long; for aluminum,

$$a_i = \frac{(11\,500)^2\,(1.26)}{1.21\,\pi\,(32\,000)^2}$$

and

$$a_i = 0.043 \text{ in.}$$

when the defect is 0.043 in. deep by 0.215 in. long.

Thus, it is apparent that for the condition imposed, the steel could tolerate a slightly larger initial defect than could the aluminum. Since the difference in the maximum allowable initial defect size is not great, the ultimate choice of a material for this situation may depend more heavily on other comparative factors, i.e., the applicability and capability of NDI techniques, the type and size of insidious defects as related to the maximum allowable initial defect size, availability, ease of fabrication, costs, etc.

2.4.2 Predicting Critical Flaw Sizes.

As mentioned in Section 2.2.3, plane-strain stress intensity (K_{Ic}) values can be obtained from several types of specimens. With valid data for a given material form, heat treatment, test temperature, and environment, critical flaw sizes can be calculated for given hardware operating stresses. The engineering usefulness of the basic stress-intensity concept in the prediction of critical flaw sizes and the use of a/Q to describe flaw size has

been supported by a number of hardware correlations, some of which are shown in Refs. 17 and 19. Comparisons between measured critical flaw sizes on test hardware and predicted critical flaw sizes based on test specimen plane-strain toughness data have shown good correlation.

From the equation shown in Fig. E2-6, it is apparent that critical flaw size is equally as dependent on applied stress as on the material fracture toughness. The following sections show approaches for calculating critical flaw sizes for the three basic types of initial flaws (surface, embedded, or through-the-thickness) based on the appropriate fracture toughness values measured from valid specimen tests.

2.4.2.1 Surface Cracks.

Calculations for surface flaws can be carried out by rearranging the stress-intensity equation developed by Irwin (Section 2.2.1),

$$(a/Q)_{cr} = \frac{1}{1.21\pi}\left(\frac{K_{Ic}}{\sigma}\right)^2$$

for a "thick-walled" structure (i.e., flaw depth less than half of the material thickness) where K_{Ic} is the plane-strain fracture toughness obtained from fracture toughness specimen tests, σ is the applied stress in structure normal to the plane of flaw, a_{cr} is the critical flaw depth, Q is the flaw shape parameter (obtained from Fig. E2-5), and $(a/Q)_{cr}$ is critical flaw size.

Since the flaw size is an unknown quantity, it is necessary to assume a flaw aspect ratio, $a/2c$, to determine Q. Using the preceding equation, the critical flaw depth, a_{cr}, can be determined for a specific value of σ and K_{Ic}.

I. Example Problem A.

Aluminum alloy 2219-T87 is selected as the material for use in a 20-in.-diam spherical gas bottle. The bottle is to operate at 4000 psig and be stored in a liquid-nitrogen propellant tank.

What is the critical flaw size?

A. Assumptions.

1. The defect is a semielliptical surface flaw with $a/2c = 0.2$.

2. The operating stress is σ = 80 percent (yield strength of the material).

B. Solution.

The yield strength and I_{Ic} values obtained from the tested specimens are as follows:

$$\sigma_{ys} = 60 \text{ ksi}$$

and

$$K_{Ic} = 37 \text{ ksi} \sqrt{\text{in.}} \quad .$$

The operating stress is

$$\sigma \approx 0.80 (\sigma_{ys}) = 0.80 (60) = 48 \text{ ksi} \quad .$$

The wall thickness required is

$$t_{req} = \frac{PR}{2\sigma} = \frac{(4000)\ (10)}{(2)\ (48\ 000)} = 0.417 \text{ in.} \quad .$$

For thick-walled structures,

$$a_{cr} = \frac{Q}{1.21\,\pi}\left(\frac{K_{Ic}}{\sigma}\right)^2 \quad ,$$

where the shape parameter Q can be found from Fig. E2-5. For this problem Q = 1.18; then

$$a_{cr} = \frac{1.18}{1.21\,(\pi)}\left(\frac{37}{48}\right)^2 = 0.184 \text{ in.}$$

and

$$2c = a/0.20 = 0.184/0.2 = 0.92 \text{ in.} \quad .$$

For surface flaws that are deep with respect to material thickness, the flaw magnification factor, M_k, can be applied to give a more accurate critical flaw size,

$$(a/Q)_{cr} = \frac{1}{1.21\,\pi}\left(\frac{K_{Ic}}{M_k\sigma}\right)^2 \quad ,$$

for thin-walled structures.

II. Example Problem B.

Use the same design that was shown in Example Problem A except that the spherical diameter of the bottle is 15 in. The wall thickness required is

$$t_{req} = \frac{PR}{2\sigma} = \frac{4000\,(7.5)}{2\,(48\,000)} = 0.313 \text{ in.}$$

For thin-walled structures,

$$a_{cr} = \frac{Q}{1.21\,\pi}\left(\frac{K_{Ic}}{M_k \sigma}\right)^2 \quad .$$

Flaw magnification factors, M_k, for the 2219-T87 aluminum are available from Fig. E2-8. Since the critical flaw depth, a_{cr}, is unknown, a "trial-and-error" iterative solution is necessary to determine the magnification factor corresponding to the critical flaw depth.

Without a magnification factor, $a_{cr} = 0.184$ in. (Example Problem A).

For $a/t = 0.184/0.313 = 0.59$, $M_k = 1.21$,

$$a_{cr} = \frac{1.18}{1.21\,\pi}\left[\frac{37}{1.21\,(48)}\right]^2 = 0.126 \text{ in.} < 0.184 \text{ in.} \quad .$$

Take an average $a = \frac{0.184 + 0.126}{2} = 0.155$ in.

For $a/t = 0.155/0.313 = 0.50$, $M_k = 1.15$,

$$a_{cr} = \frac{1.18}{1.21\,\pi}\left[\frac{37}{1.15\,(48)}\right]^2 = 0.139 \text{ in.} < 0.155 \text{ in.} \quad .$$

Take an average $a = \frac{0.155 + 0.139}{2} = 0.147$ in.

For $a/t = 0.147/0.313 = 0.47$, $M_k = 1.13$,

$$a_{cr} = \frac{1.18}{1.21\,\pi}\left[\frac{37}{1.13\,(48)}\right]^2 = 0.144 \approx 0.147 \text{ in.} \quad .$$

Further reiteration will provide more accuracy if desired.

If adequate flaw magnification values are not available for a particular material, a reasonable estimate for M_k is the approximate Kobayashi solution shown in Fig. E2-25. However, it should be understood that its use can result in somewhat conservative answers for more ductile materials and perhaps unconservative answers for more brittle materials.

2.4.2.2 Embedded Flaws.

The calculations for embedded flaws in thick-walled structures will be the same as for surface flaws except that a_{cr} is the one-half critical flaw depth of the embedded flaw, and the correction factor of 1.21 for the effect on stress intensity of the stress-free surface (Section 2.2.1) is eliminated. Thus the equation for one-half critical internal flaw size is

$$(a/Q)_{cr} = \left(\frac{1}{\pi} \frac{K_{Ic}}{\sigma}\right)^2 .$$

Although flaw magnification effects have been studied for deep surface flaws, apparently no similar research has been done for internal flaws with large flaw-depth-to-material-thickness ratios. The fact that internal flaws are hidden, making their size difficult if not impossible to accurately determine, presents a problem in the study of internal flaw magnification effects. The assumption might be made that the same flaw magnification factors, M_k, used for deep surface flaws might be applied to the equation for critical embedded flaw sizes. However, there is no evidence of how conservative or unconservative this assumption is.

On the other hand, to account for the lack of knowledge about flaw geometry and orientation, it can be conservatively assumed that flaws are surface (or barely subsurface) flaws and that they are long in relation to depth ($Q \approx 1.0$).

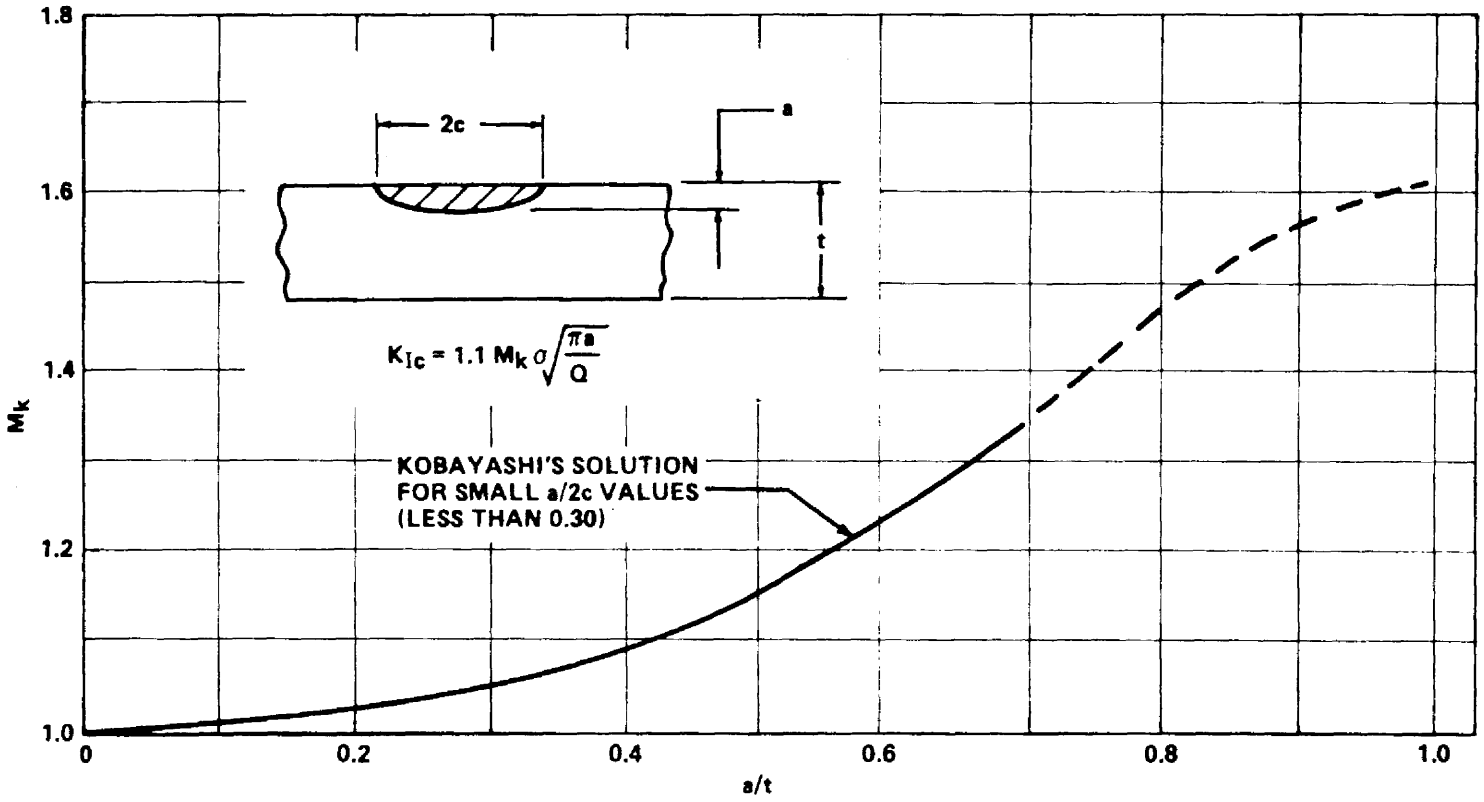

FIGURE E2-25. STRESS-INTENSITY MAGNIFICATION FACTORS FOR DEEP SURFACE FLAWS

2.4.2.3 Through-the-Thickness Cracks.

To calculate through-the-thickness critical crack length, the basic plane stress equation for through-the-thickness cracks in an infinitely wide plate (Section 2.2.2.1) can be rearranged to give

$$\ell_{cr}/2 = \frac{1}{\pi}\left(\frac{K_c}{\sigma}\right)^2 - \frac{1}{2\pi}\left(\frac{K_c}{\sigma_{ys}}\right)^2 ,$$

where K_c is the plane stress fracture toughness obtained from an edge-notched or center-cracked specimen, σ is the applied stress in the structure normal to the plane of the crack, σ_{ys} is the tensile yield strength of the material, and ℓ_{cr} is the critical crack length.

I. Example Problem A.

Aluminum alloy 2219-T87 is selected as the material for use in a 15-in. diameter compressed air cyclinder. The cylinder is to operate at 1000 psig in ambient room atmosphere.

What is the critical flaw size?

A. Assumptions.

1. The defect is a semielliptical surface flaw with $a/2c = 0.2$.

2. The operating stress is σ = 80 percent of material yield strength.

B. Solution.

The yield strength and K_{Ic} values obtained from test specimens are as follows:

σ_{ys} = 50 ksi

and

$$K_{Ic} = 32 \text{ ksi } \sqrt{\text{in.}} \quad .$$

An estimate of K_c versus material thickness based on 2219-T87 test specimens is shown in Fig. E2-26 (Refs. 20 and 21).

The operating stress is

$$\sigma = 0.80 (\sigma_{ys}) = 0.80 (50) = 40 \text{ ksi} \quad .$$

The wall thickness required is

$$t_{req} = \frac{PR}{\sigma} = \frac{1000 (7.5)}{40\,000} = 0.188 \text{ in.} \quad .$$

For thick-walled structures,

$$a_{cr} = \frac{Q}{1.21 \pi} \left(\frac{K_{Ic}}{\sigma} \right)^2 \quad .$$

From Fig. E2-5, $Q = 1.18$; then

$$a_{cr} = \frac{1.18}{1.21 \pi} \left(\frac{32}{40} \right)^2 = 0.199 > 0.188 \text{ in.} \quad .$$

Therefore, the critical flaw is apparently a through-the-thickness crack and the tank will leak before failure. The critical crack length of failure is predicted to be

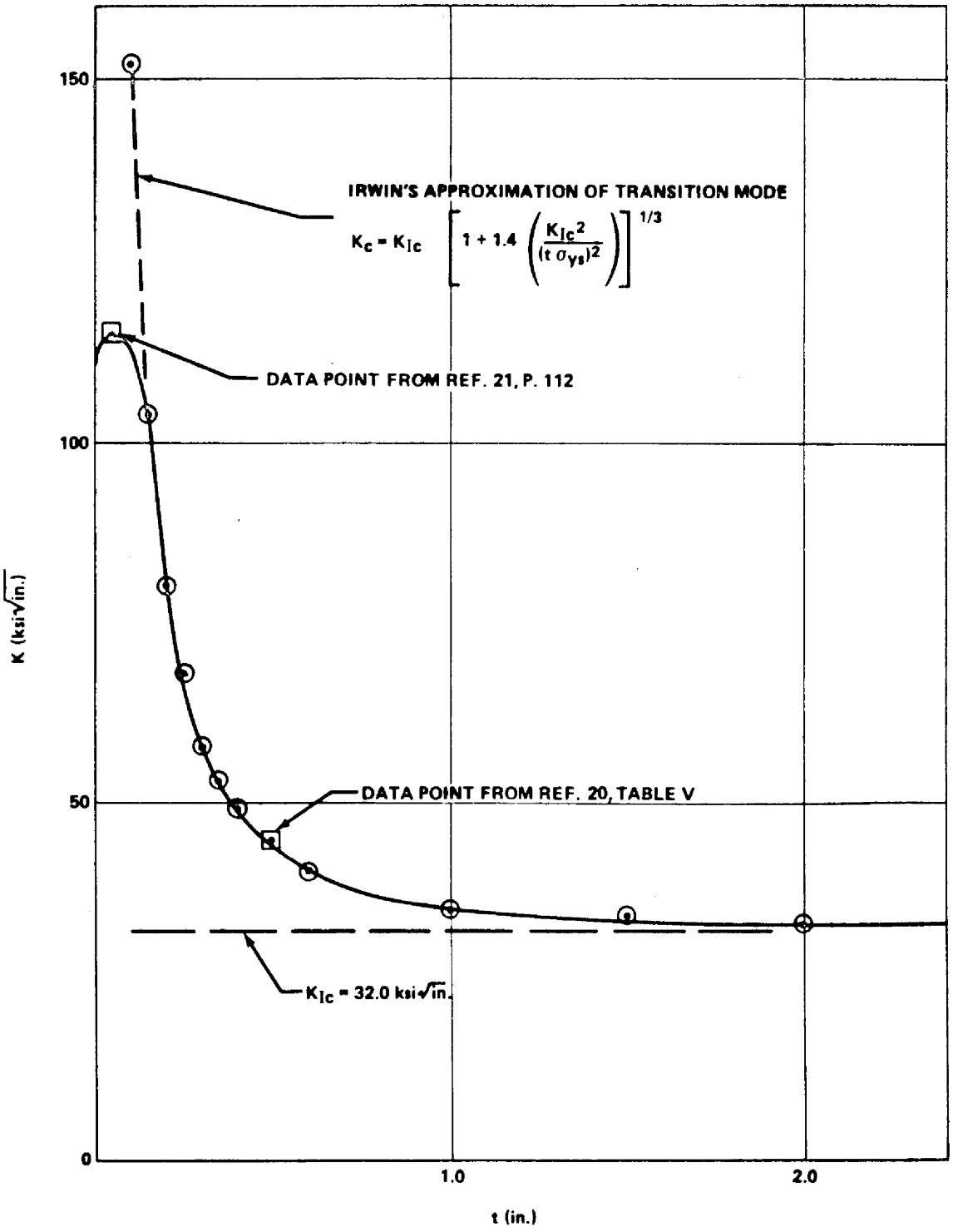

FIGURE E2-26. ESTIMATE OF K_c VERSUS t FOR 2219-T87 ALUMINUM ($T = 70°F$, $K_{Ic} = 32.0$ ksi $\sqrt{\text{in.}}$)

$$\ell_{cr} = \frac{2}{\pi}\left(\frac{K_c}{\sigma}\right)^2 - \frac{1}{\pi}\left(\frac{K_c}{\sigma_{ys}}\right)^2 \quad .$$

The plane-stress fracture toughness value, K_c, from Fig. E2-26, is 84 ksi $\sqrt{\text{in.}}$

$$\ell_{cr} = \frac{2}{\pi}\left(\frac{84}{40}\right)^2 - \frac{1}{\pi}\left(\frac{84}{50}\right)^2 = 2.81 - 0.91 = 1.90 \text{ in.} \quad .$$

2.4.3 Structure Design.

2.4.3.1 Service Life Requirements and Predictions.

With pressure cycles and time at stress, an initial flaw or defect in a structure will grow in size until it attains the critical size at the applied operating stress level, and failure will result. The flaw-growth potential (in inches) is equal to the critical size minus the initial size. The life of the structure directly depends upon this flaw-growth potential and the subcritical flaw-growth characteristics of the material.

The determination of the initial flaw sizes generally relies upon the use of NDI procedures; however, the conventional proof test can be considered to be one of the most positive inspection procedures available. A successful proof test actually defines the maximum possible initial flaw size that exists in the vessel. This results from the functional relationship between stress level and flaw size as defined by the critical stress intensity (K_{Ic}) and illustrated in Fig. E2-6.

Probably the most predominant types of subcritical flaw growth are fatigue growth resulting from cyclic stress and environmentally induced sustained stress growth. Also, growth may occur even in the absence of severe environmental effects if the initial flaw size approaches the critical flaw size.

The technique used for predicting the subcritical cyclic or sustained stress flaw growth makes use of fracture specimen testing and the stress-intensity concept.

It has been shown (Refs. 6 and 17) that the time or cycles to failure at a given maximum applied gross stress level depends on the magnitude of the initial stress intensity at the flaw tip, K_{Ii}, compared with the critical stress intensity, K_{Ic} [that is, cycles or time to failure = f (K_{Ii}/K_{Ic})]. Also, it is seen that the ratio of initial flaw size to critical flaw size is related to the stress-intensity ratio as follows:

$$\left(\frac{K_{Ii}}{K_{Ic}}\right)^2 = \frac{\frac{a_i}{Q_i}}{\frac{a_{cr}}{Q_{cr}}} \quad .$$

Thus, if cyclic or sustained stress fracture specimens are used to obtain experimentally the K_{Ii}/K_{Ic} versus cycles or time curves for a material, the cycles or time required for any given initial flaw to grow to critical size can be predicted. Conversely, if the required life of the structure is known in terms of stress cycles or time at stress, the maximum allowable initial flaw size can be determined.

The cyclic flaw-growth data are plotted in terms of stress-intensity ratio, K_{Ii}/K_{Ic}, versus log of cycles, as shown schematically in Fig. E2-27a. By squaring the ordinate value, the plot of the ratio of initial flaw size to critical flaw size versus the log of cycles (Fig. E2-27b) can be obtained. It should also be recognized that flaw size can be determined after any incremental number of cycles. For example, if the initial flaw-size ratio was 0.40, the flaw would have grown in A cycles, increasing the ratio to 0.6; in B cycles, it would have grown to 0.8, etc.

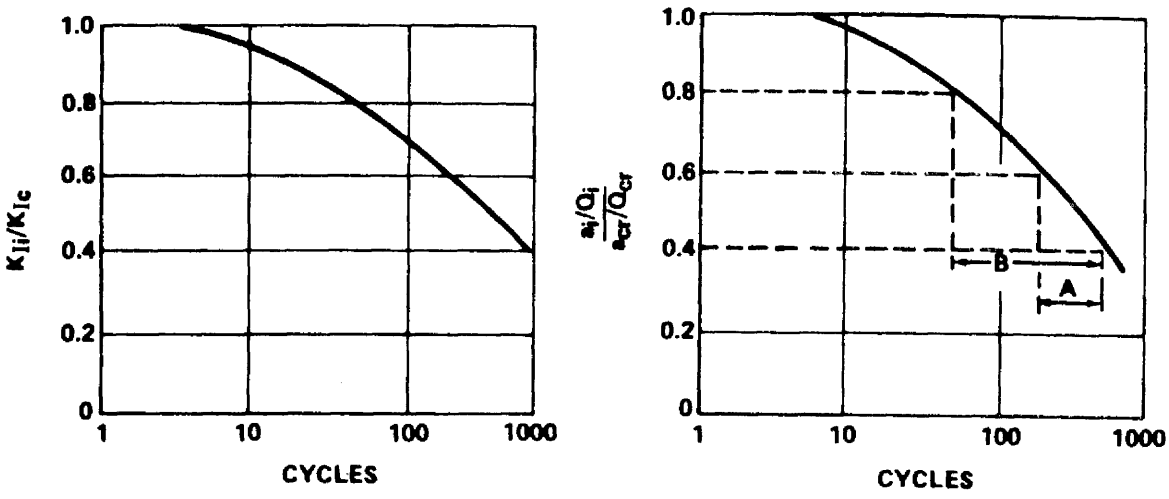

FIGURE E2-27. SCHEMATIC REPRESENTATION OF CYCLIC FLAW GROWTH

Cyclic flaw-growth data have been obtained on a number of materials used in the aerospace industry. Some such data are shown in Figs. E2-28 and E2-29.

The application of fracture-specimen testing to define the effects of sustained load on flaw growth is essentially the same as used in defining cyclic flaw growth. A constant load is applied to a flawed specimen such that the initial stress intensity is less than the critical value and the time to failure is recorded. The K_{Ii}/K_{Ic} values are computed and the K_{Ii}/K_{Ic} ratio is plotted versus log of time to failure.

Plots of K_{Ii}/K_{Ic} versus log of time for most materials indicate the existence of a threshold stress-intensity level below which sustained stress growth does not occur. Figure E2-30 shows data for 17-7 PH steel tested in both dry and wet environments, and Fig. E2-31 shows surface-flawed specimen data for 2219-T87 aluminum tested in liquid nitrogen. In neither case does it seem that the environment played an important role in the sustained stress growth. In both cases the apparent threshold stress-intensity levels are quite high.

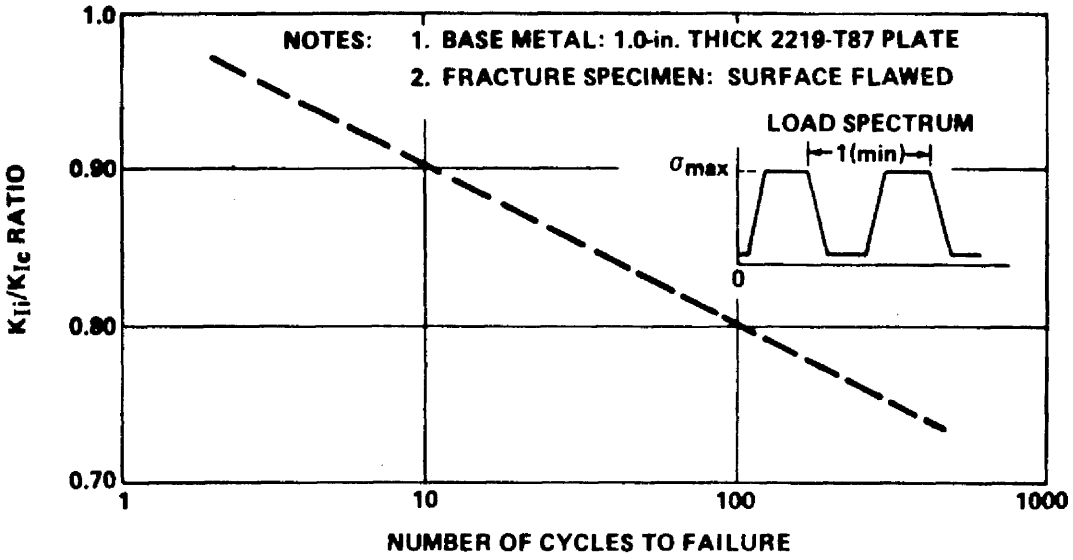

FIGURE E2-28. BASE METAL CYCLIC FLAW-GROWTH DATA (-320 °F, LONGITUDINAL GRAIN)

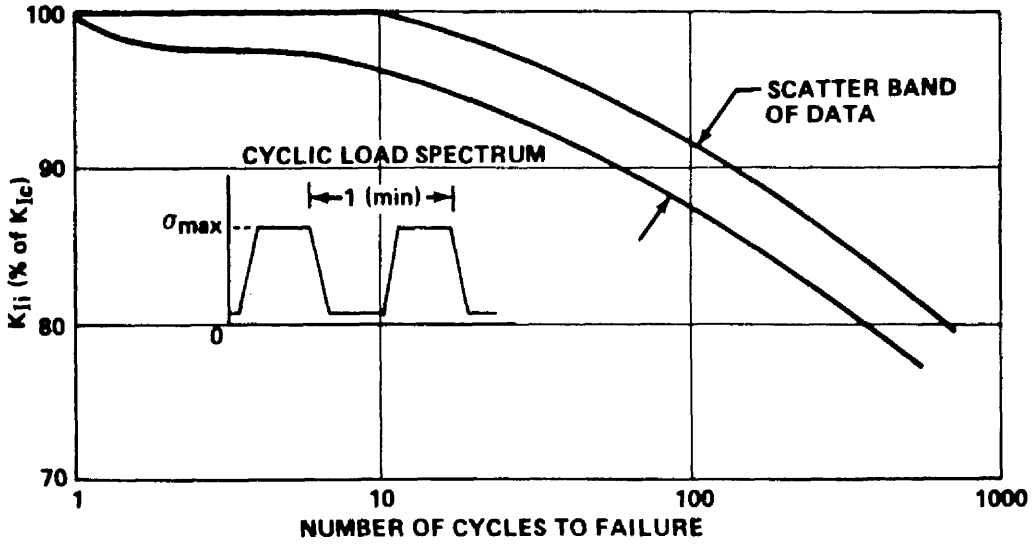

FIGURE E2-29. CYCLIC FLAW-GROWTH DATA OF 6Al-4V TITANIUM PLATE TESTED AT -320 °F

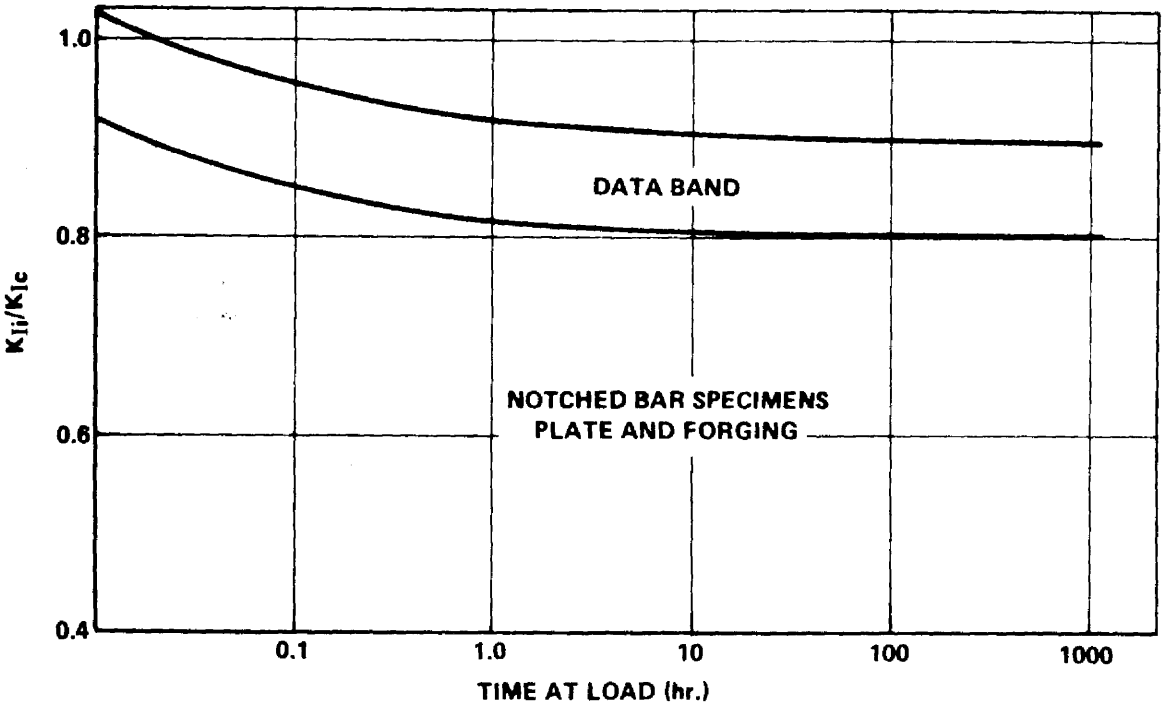

FIGURE E2-30. SUSTAINED STRESS FLAW-GROWTH DATA FOR ROOM-TEMPERATURE TESTS OF 17-7 PH STEEL

Let us now consider the significance of sustained stress flaw growth and specifically the threshold stress-intensity concept on the estimated total cyclic life of a tension-loaded structure containing an initial crack or crack-like flaw. To illustrate this, the schematic representation of the K-N curve is reconstructed in Fig. E2-32, but superimposed on this curve is a horizontal like at $K_{Ii}/K_{Ic} = 0.80$. This is assumed to be the threshold stress intensity. Now consider the situation where the initial flaw size and applied cyclic stress result in an initial stress intensity equal to 50 percent of the critical value. From the curve, it is seen that it would take a total of A cycles to grow this initial flaw to critical size and cause failure. However in B cycles, the initial flaw would have increased in size enough to cuase the stress intensity to reach the threshold value of $K_{Ii}/K_{Ic} = 0.80$. With additional cycles the

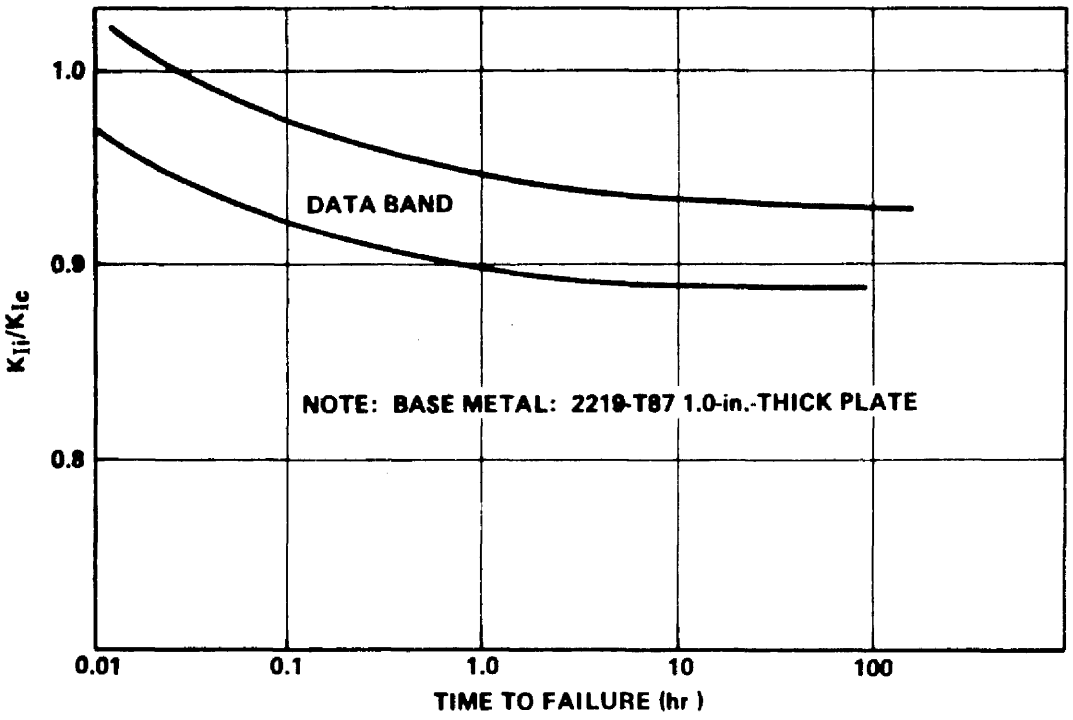

FIGURE E2-31. SUSTAINED STRESS FLAW-GROWTH DATA FOR 2219-T87 ALUMINUM AT -320 °F

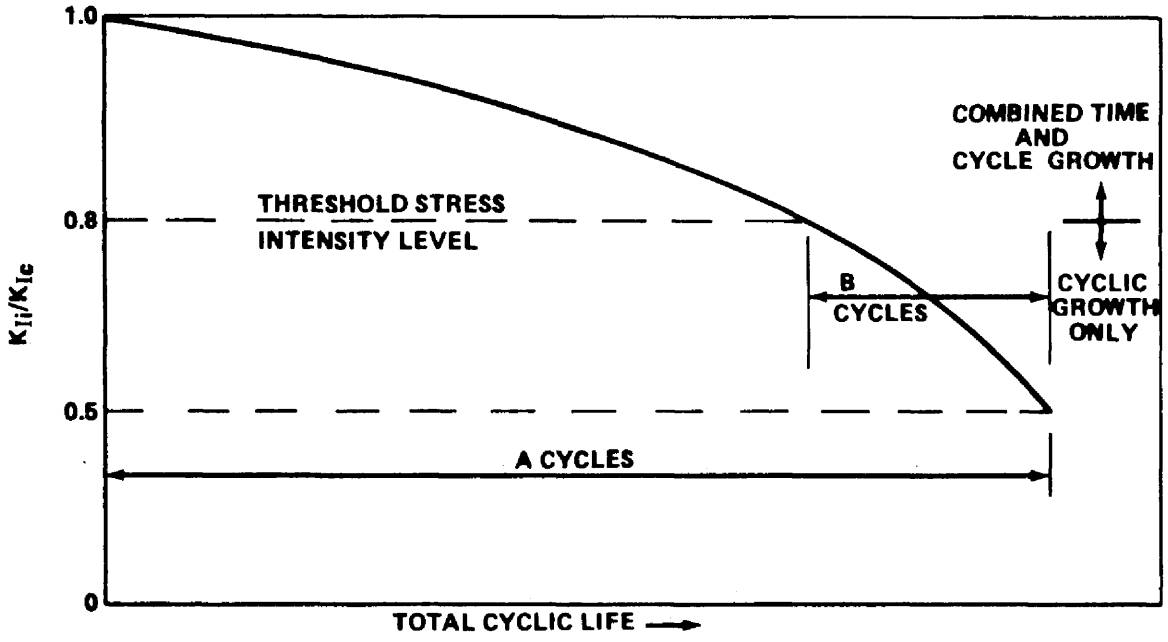

FIGURE E2-32. COMBINED CYCLIC AND SUSTAINED STRESS FLAW GROWTH SCHEMATIC INTERPRETATION

stress intensity would further increase and, if the stress were sustained sufficiently long, it appears possible that failure could occur on the (B + 1) cycle.

If, on the other hand, the cycles were applied with little time at maximum cyclic stress, it appears that the total of A cycles could be realized. It is hypothesized that below the threshold K-value, the time at sustained stress has little or no effect on cyclic life. Above the threshold value there will be an interaction such that failure could occur anywhere within the range of (B + 1) to A cycles, depending on the time the maximum stress is held during each cycle. The development of the exact time-cycle interaction curves above the threshold value would be a complex and expensive task and, as applied to most tankage structure, may not be of great importance. It appears more rational to determine the basic cyclic data and the threshold-intensity values and then verify (through prolonged-time specimen cyclic tests) that time at load is not of major significance below the threshold value. In the application of the data to fatigue-life estimation, the maximum allowable stress intensity would be limited to the threshold value as determined for the material in question and for the applicable service environment. If the threshold is very low, steps should be taken to protect the material from the environment.

The operational cyclic life of pressure vessels can be determined if the following data are available:

1. Proof-test factor α.
2. Maximum design operating stress σ_{op}.
3. Fracture toughness K_{Ic}.
4. Experimental cyclic and sustained stress flaw growth for the vessel material.

If the cycles to be applied to the vessel have short hold time at the maximum stress σ_{op}, the stress intensity at σ_{op} can be allowed to reach the critical value K_{Ic} and therefore the allowable flaw growth potential is $a_{cr} - a_i$. For long hold times at the maximum stress, the stress intensity could not be allowed to exceed the sustained stress threshold value K_{TH} and the allowable flaw growth potential is $a_{th} - a_i$. Typical threshold stress-intensity data can be obtained from Refs. 12 and 22.

I. Example Problem A (Thick-Walled Vessel).

Cyclic life prediction can be made by utilizing the proof-test factor and the relationships between K_{Ii}/K_{Ic} and cycles to failure for various values of R (ratio of minimum to maximum stress during a cycle) for the material-environment combination.

The procedure for assessing the structural integrity of the thick-walled vessels follows. In the first analysis for the assessment of the structural integrity of the thick-walled vessel, it is always assumed that all the pressure cycles are applied at $R = 0$. Since the analysis based on $R = 0$ will always show the remaining cyclic life less than that based on the analysis of $R \neq 0$ (actual R ratios), the prediction of cyclic life based on the analysis of $R = 0$ is invariably conservative. If the pressure vessel is shown unsatisfactory for the flight based on $R = 0$, then the prediction analysis for the remaining cyclic life is conducted based on the actual R values at which the cycles are applied. An excellent illustrative example abstracted from Ref. 12 is given as follows.

Suppose that a thick-walled 6Al-4V (STA) titanium helium tank is successfully proof tested at a proof-test factor of 1.50 times the maximum design operating stress. Suppose that the proof-tested tank is subjected to the following pressure cycles before the flight, as shown in Fig. E2-33:

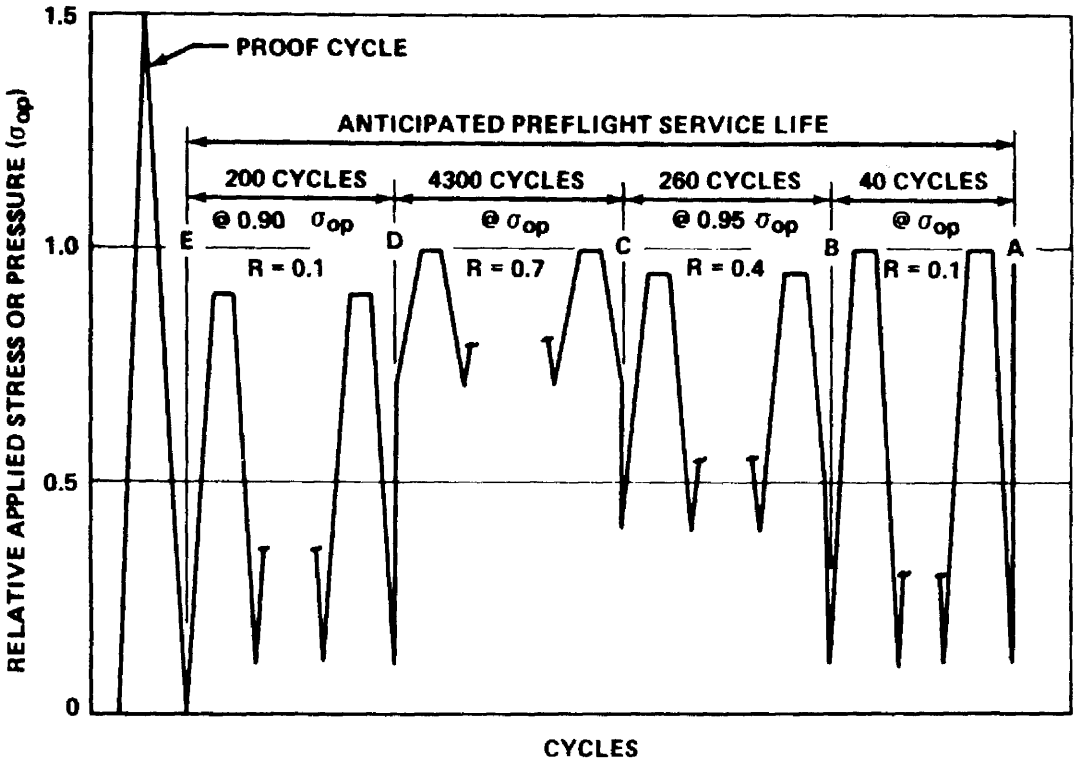

FIGURE E2-33. CYCLIC HISTORY OF A THICK-WALLED VESSEL (EXAMPLE PROBLEM A)

1. 200 loading cycles with the maximum stress as 90 percent of σ_{op} and R = 0.1.

2. 4300 loading cycles with the maximum stress as σ_{op} and R = 0.7.

3. 260 loading cycles with the maximum stress as 95 percent of σ_{op} and R = 0.4.

4. 40 loading cycles with the maximum stress as σ_{op} and R = 0.1.

The cyclic life curves for 6Al-4V (STA) titanium for the environment of room-temperature air are reproduced for R = 0.0, R = 0.1, R = 0.4, and R = 0.7 in Fig. E2-34. The difference between the plots of cyclic life against K_{Ii}/K_{Ic} for R = 0 and R = 0.1 is negligible for this material-environment

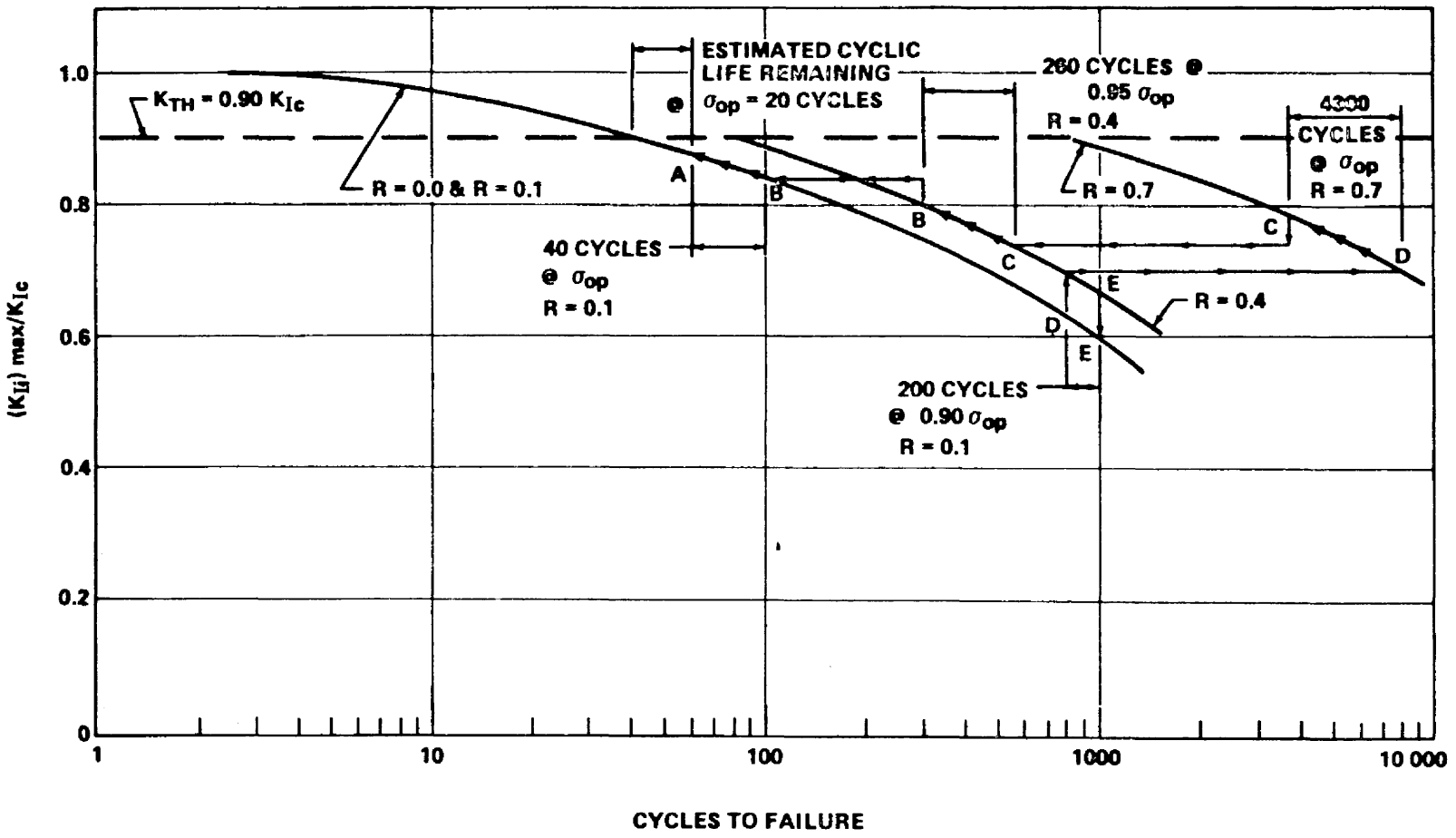

FIGURE E2-34. PREDICTION OF CYCLIC LIFE OF A THICK-WALLED VESSEL (EXAMPLE PROBLEM A)

combination, and hence both are shown by the same plot in Fig. E2-34. The threshold stress-intensity level for the material in the environment of room-temperature air is 90 percent of K_{Ic}.

The maximum possible K_{Ii}/K_{Ic} ratio that could exist in the vessel after the proof test at σ_{op} is $1/\alpha = 0.667$. It can be seen from the $R = 0$ plot in Fig. E2-34 that the maximum cycles to failure are about 600 at σ_{op} if the hold times at maximum stress are small. If the analysis is based on $R = 0$ instead of actual R, the pressure-cycle history shows that the vessel is critical. In the following, the assessment of the vessel is made based on the appropriate values of R.

At the beginning of 200 loading cycles with the maximum stress as $0.90\ \sigma_{op}$, the maximum K_{Ii}/K_{Ic} is given by $0.90 \times 0.667 = 0.60$. This point is indicated by E on $R = 0.1$ curve. The 200 loading cycles of $0.90\ \sigma_{op}$ and $R = 0.1$ change the K_{Ii}/K_{Ic} ratio from Point E to Point D on the plot of $R = 0.1$. The K_{Ii}/K_{Ic} ratio at the end of 200 loading cycles of $R = 0.1$ is 0.63.

The stress is increased by 10 percent at the end of 200 cycles. Hence, the K_{Ii}/K_{Ic} ratio at the beginning of 4300 cycles at σ_{op} and $R = 0.7$ is $(1.0/0.9) \times 0.63 = 0.70$. This is shown by Point D on the plot of $R = 0.7$. The 4300 loading cycles at σ_{op} and $R = 0.7$ change the K_{Ii}/K_{Ic} ratio from Point D to Point C on the plot of $R = 0.7$, where its value is 0.78.

The stress is decreased by 5 percent at the end of 4300 cycles. Hence, the K_{Ii}/K_{Ic} ratio at the beginning of 260 cycles at $0.95\ \sigma_{op}$ is $(0.95/1.0) \times 0.78 = 0.74$, which is shown by Point C on the $R = 0.4$ plot. The 260 cycles at $0.95\ \sigma_{op}$ and $R = 0.4$ change the K_{Ii}/K_{Ic} ratio from Point C to Point B on the $R = 0.4$ plot, where its value is 0.80.

The stress is increased by 5 percent at the end of 260 cycles. Hence, the K_{Ii}/K_{Ic} ratio at the beginning of 40 cycles at σ_{op} is $(1.0/0.95) \times 0.80 = 0.84$, which is illustrated by Point B on the $R = 0.1$ plot. The 40 cycles at σ_{op} and $R = 0.1$ increase the K_{Ii}/K_{Ic} ratio from 0.84 to 0.875, which is shown by Point A in Fig. E2-34.

Since the stress intensity at the end of 40 cycles at σ_{op} is less than the threshold stress intensity, the vessel is considered to be safe for the flight. It will take 20 loading cycles at σ_{op} and $R = 0.1$ to increase K_{Ii}/K_{Ic} from 0.875 to 0.90. Thus, the estimated minimum cyclic life remaining for the vessel is 20 cycles.

II. Example Problem B (Thin-Walled Vessel).

In thin-walled vessels the flaw depth becomes deep with respect to the wall thickness prior to reaching the critical size. Therefore, Kobayashi's magnification factor for deep surface flaws M_k must be considered. In thin-walled vessels it is assumed that the flaws are long with respect to their depth and, consequently, Q is assumed to be equal to unity in the Kobayashi equation.

To determine the cyclic life of a thin-walled vessel, the following relations are required (Ref. 22).

1. Proof-test factor, σ_{op}, K_{Ic}, and K_{TH}.

2. The σ versus a curve, similar to Fig. E2-35, to determine the flaw size, a_i, a_{cr}, and a_{Th}. The curve is obtained from the following equation:

$$\sigma = \frac{K_I}{(1.1\, M_k \sqrt{\pi a})} \quad .$$

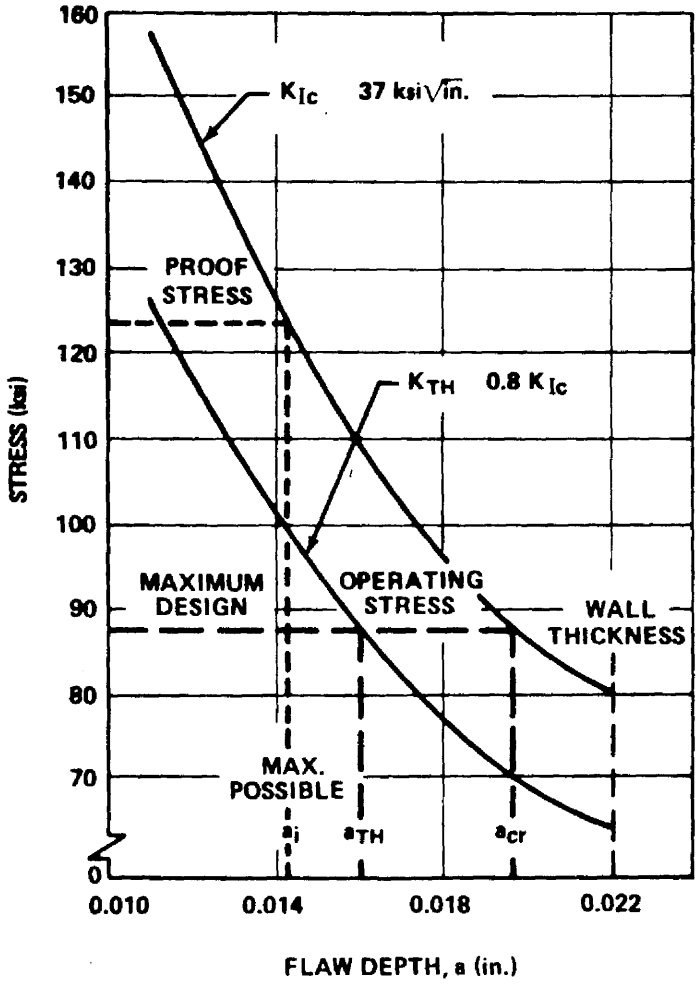

FIGURE E2-35. DETERMINATION OF INITIAL AND CRITICAL FLAW SIZES

3. The K_{Ii}/K_{Ic} versus flaw growth rate da/dN to determine the flaw growth rate at any stress level. The flaw growth rates can be obtained by differentiating the K_{Ii}/K_{Ic} versus cycles to failure curve, similar to that of Fig. E2-36 (Ref. 22). This curve is obtained from the specimens where a_{cr}/t is less than half. For an assumed maximum cyclic stress level, say σ_1, the given K_{Ii}/K_{Ic} versus N curve can be converted to an a/Q versus N curve by the equation

$$a/Q = \frac{1}{1.21\,\pi}\left(\frac{K_{Ii}}{\sigma_1}\right)^2 \quad .$$

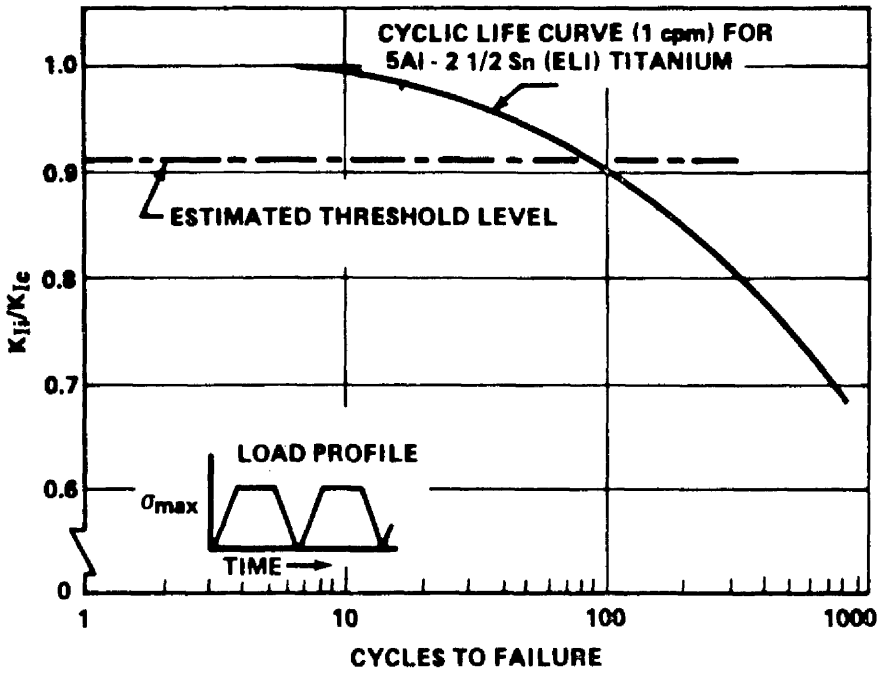

FIGURE E2-36. COMBINED SUSTAINED AND CYCLIC STRESS LIFE DATA [5 Al — 2 1/2 Sn (ELI) TITANIUM AT -320°F]

The slope of the a/Q versus N curve gives the plot for the flaw growth rate d/dN (a/Q) versus K_{Ii}/K_{Ic} for the stress level σ_1. From the preceding equation for a given K_{Ii}, a/Q at the stress level σ_2 is related with a/Q at σ_1 as

$$(a/Q)\sigma_2 = \left(\frac{\sigma_1}{\sigma_2}\right)^2 \left(\frac{a}{Q}\right) \sigma_1 \quad .$$

From this equation it can be concluded that the flaw growth rate at any stress level σ_2 is related to the growth rate at σ_1 as follows:

$$[d/dN\ (a/Q)]\ \sigma_2 = (\sigma_1/\sigma_2)^2\ [d/dN\ (a/Q)]\ \sigma_1 \quad .$$

The prediction of the remaining cycle life and the structural integrity of the thin-walled vessel is demonstrated by an illustrative example abstracted from Ref. 22 and is given as follows.

Suppose that a thin-walled 6Al-4V titanium (STA) propellant tank containing N_2O_4 at room temperature is successfully proof tested with water at room temperature to a proof-test factor of 1.41 times the maximum design operating stress, σ_{op}. Suppose that the proof-tested tank is subjected to the following pressure cycles before the flight:

1. Twenty loading cycles with the maximum stress as 90 percent of σ_{op}.

2. Twelve loading cycles with the maximum stress as 95 percent of σ_{op}.

3. Five loading cycles with the maximum stress as σ_{op}.

It is desired to assess the structural integrity of the pressure vessel from the fracture mechanics standpoint and estimate the minimum cyclic life remaining for the vessel at σ_{op}. This example is treated with specific numbers since the stress-intensity factor has to be corrected for the a/t ratio according to Fig. E2-25. The thickness of the tank is 0.022 in. The maximum design operating stress, σ_{op}, is 87.5 ksi. The material of this gage under the above-mentioned environmental conditions has the minimum fracture toughness of 37 ksi $\sqrt{\text{in.}}$ and the threshold stress intensity of 80 percent of K_{Ic}.

The σ versus a plots are given for K_{Ic} and $K_{TH} = 0.80\ K_{Ic}$ in Fig. E2-35. Since the proof stress is $1.41 \times \sigma_{op} = 123.6$ ksi, it is clear from Fig. E2-35 that the maximum possible a_i that could exist is 0.0143 in. Here it is assumed that the depressurization from the proof pressure is

rapid enough so that no significant flaw growth occurs during the depressurization. Also, as shown in Fig. E2-35, for the stress level of σ_{op}, a_{cr} is 0.0196 in. and a_{TH} is 0.0160 in.

The plot of the K_{Ii}/K_{Ic} versus flaw growth rate for 6AL-4V titanium at room temperature is reproduced in Fig. E2-37 for σ = 100 ksi. The 99-percent confidence level flaw growth rate curve is obtained from the cyclic data of R = 0.0; it is assumed in this example that all the cycles are applied at R = 0.0.

Taking into account the effect of stress level on the flaw growth rates, the rates are arithmetically integrated from a_i = 0.0143 in. to a_{cr} = 0.0196 in. according to Fig. E2-38 to calculate the cycles to failure for the stress level of σ_{op}. The plot of flaw depth against cycles to failure for the stress level of σ_{op} is shown in Fig. E2-39.

When the maximum cyclic stress is 0.95 σ_{op}, a_i is still 0.0143 in. but a_{cr} is 0.0208 in. and a_{TH} = 0.0167 in. from Fig. E2-35. Based on the stress level of 0.95 σ_{op}, the flaw growth rates are integrated from a_i = 0.0143 in. to a_{cr} = 0.208 in. to calculate the cycles to failure. A similar procedure is followed to obtain the relation of flaw depth against cycles to failure for the stress level of 0.90 σ_{op}. These plots are shown in Fig. E2-39.

At the end of the proof cycle and the beginning of the first cycle at the maximum cyclic stress of 0.90 σ_{op}, the maximum possible flaw depth is 0.0143 in. This is shown by Point D in Fig. E2-39. The 20 loading cycles with the maximum stress as 0.90 σ_{op} change a from Point D to Point C on the plot of 0.90 σ_{op} (Fig. E2-39).

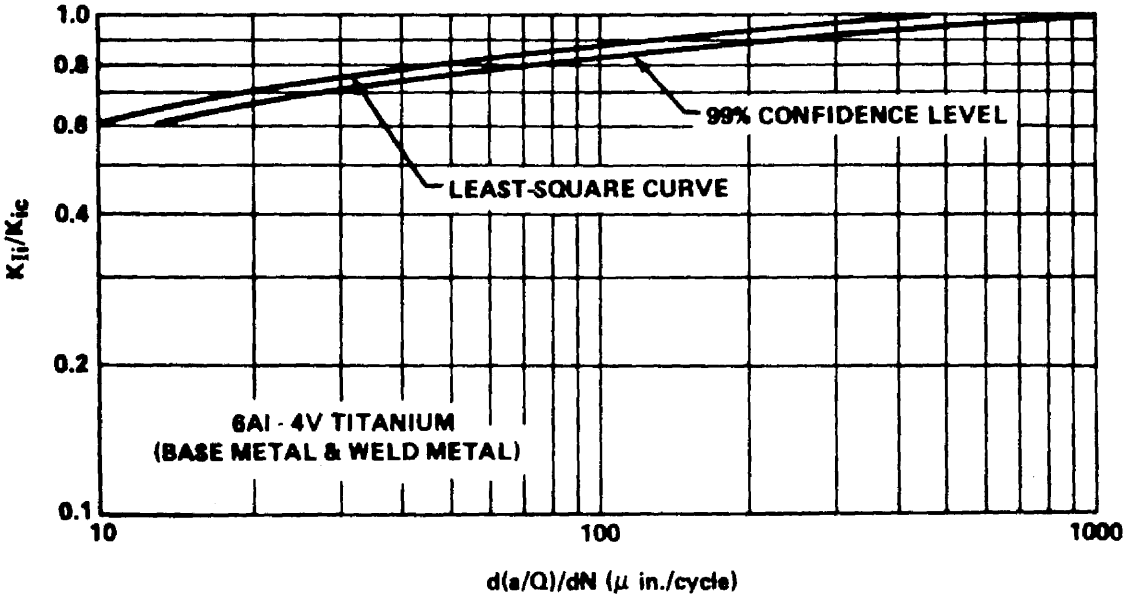

FIGURE E2-37. CYCLIC FLAW-GROWTH RATES
(FOR σ_{max} = 100 ksi)

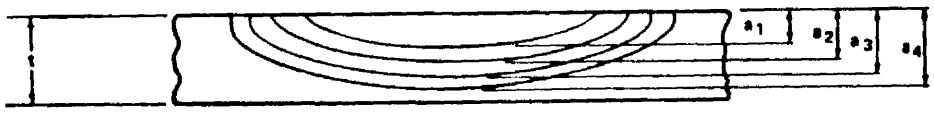

a	Δa	a/t	M_k[a]	K[b]	MEAN K	MEAN[c] da/dN	ΔN	N
a_1	$a_2 - a_1$	a_1/t	M_{k1}	K_1	$\frac{K_1 + K_2}{2}$	da_{1-2}/dN	ΔN_1	ΔN_1
a_2	$a_3 - a_2$	a_2/t	M_{k2}	K_2	$\frac{K_2 + K_3}{2}$	da_{2-3}/dN	ΔN_2	$\Delta N_1 + \Delta N_2$
a_3								$\Delta N_1 + \Delta N_2 + \Delta N_3$

a. Obtain from Kobayashi's solution of M_k vs a/t

b. $K = 1.1\sqrt{\pi}\,\sigma\,(a)^{1/2}\,M_k$

c. Obtain from basic K vs da/dN curve.

FIGURE E2-38. ARITHMETIC INTEGRATION OF FLAW-GROWTH-RATE DATA (DEEP FLAWS IN THIN-WALLED VESSELS)

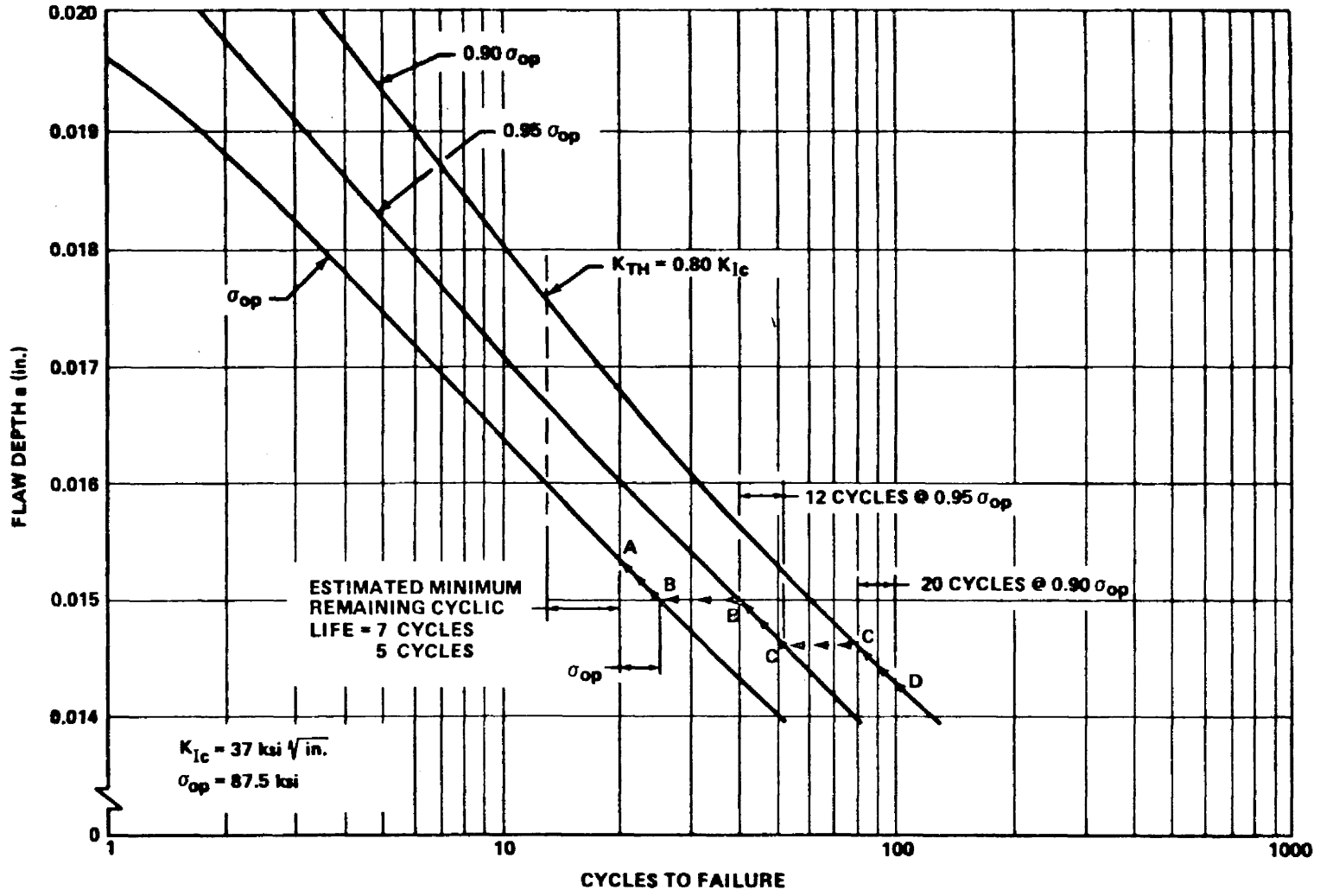

FIGURE E2-39. PREDICTION OF CYCLIC LIFE OF A THIN-WALLED VESSEL (ILLUSTRATIVE EXAMPLE)

The tank-wall stress is increased by 5 percent at the end of 20 loading cycles with the maximum stress as 0.90 σ_{op}. The flaw size remains the same during the stress increase. This is shown by Point C on the plot of 0.95 σ_{op} in Fig. E2-39.

The 12 loading cycles with the maximum stress as 0.95 σ_{op} change a from Point C to Point B on the plot of 0.95 σ_{op} in Fig. E2-39.

At the end of 12 loading cycles with the maximum stress as 0.95 σ_{op}, the stress is increased by 5 percent. This is shown by Point B on the plot of σ_{op} in Fig. E2-39.

The five loading cycles with the maximum stress as σ_{op} change a from Point B to Point A on the plot of σ_{op} in Fig. E2-39. The flaw depth at A is 0.01534 in. This is smaller than a_{TII}, which is 0.0160 in. Hence the vessel is considered to be safe for the flight. Also from Fig. E2-39, it will take seven cycles at σ_{op} to increase the flaw depth from 0.01534 in. to 0.0160 in. Hence, the minimum estimated cyclic life remaining for the vessel is seven cycles.

2.4.3.2 Allowable Initial Flaw Size.

Allowable initial flaw sizes in a designed structure depend on the service life requirements for the structure and fracture toughness properties of the material selected. The prevention of failure requires that either the actual initial flaw sizes or the maximum possible initial flaw size be known. Nondestructive inspection provides the only means of determining actual initial flaw sizes. A successful proof test specifies the maximum possible initial flaw size which can exist after the proof test and, in turn, provides the maximum possible initial to critical stress-intensity ratio, K_{Ii}/K_{Ic}. To determine the maximum allowable initial flaw size, the initial to critical stress-intensity ratio, based on the service life requirements, must be determined.

The calculation of allowable initial flaw size is demonstrated by the following example.

I. Example Problem A.

A cyclic loaded pressure vessel of aluminum alloy must meet the following design conditions:

1. Required minimum life, 40 000 cycles.
2. Maximum stress in a cycle 1/2 σ_{ys} = 35 000 psi.
3. K_{Ic} of weld metal = 15 000 psi $\sqrt{\text{in.}}$
4. Semielliptical surface defect (length 4 × depth).

What is the allowable initial flaw size which will grow to a critical size in 40 000 cycles?

Solution.

From Fig. E2-40 (Ref. 18), the K_{Ii}/K_{Ic} ratio corresponding to 40 000 cycles of life is 0.36. The initial stress intensity can now be determined:

$$K_{Ii}/K_{Ic} = 0.36 = \frac{K_{Ii}}{15\ 000}$$

and

$$K_{Ii} = 0.36\ (15\ 000) = 5400 \text{ psi } \sqrt{\text{in.}} \quad .$$

Knowing the design stress of 35 000 and the expression of the type of defect, it is now possible to find the defect size corresponding to a K_{Ii} of 5400 psi $\sqrt{\text{in.}}$:

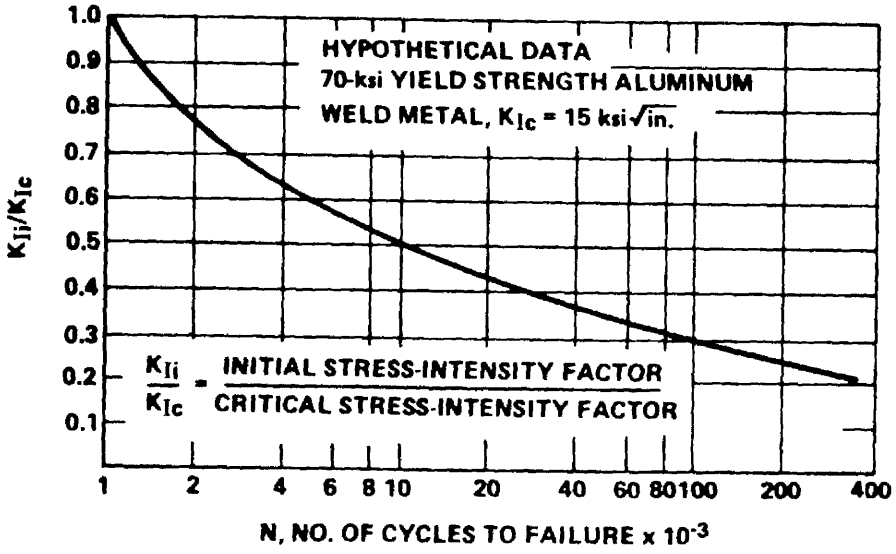

FIGURE E2-40. CYCLIC FLAW-GROWTH DATA FOR ALUMINUM ALLOY

$$a_i = \frac{K_{Ii}^2 Q}{1.21 \pi \sigma^2} = \frac{(5400)^2 (1.4)}{1.21 \pi (35\,000)^2} = 0.0088 \text{ in.}$$

The value of $Q = 1.4$ is taken from Fig. E2-5 for $a/2c = 1/4 = 0.25$ and $\sigma/\sigma_{ys} = 1/2 = 0.50$.

$$2c_i = 4a_i = 4\,(0.0088) = 0.0352 \text{ in.}$$

Therefore, the size of an initial flaw which will just grow to a critical size in 40 000 cycles is 0.0088 in. deep by 0.0352 in. long.

2.4.3.3 Nondestructive Inspection Acceptance Limits.

The NDI requirements for any given structure are a function of the allowable flaw sizes. They are limited by any economic or schedule implications associated with a proof-test failure and by the reliability of the

inspection techniques for detecting initial flaws. Allowances should be made for any lack of specific knowledge of flaw geometry and orientation. When there is a lack of flaw definition, the worst possible flaw geometry and orientation might be assumed.

Also, in arriving at acceptance limits, the allowable spacing for internal or surface flaws (that is, aligned flaws in weldments) must be considered. An approximate analytical solution for the interaction of elliptically shaped coplanar flaws has been obtained by Kobayashi and Hall (Ref. 23). The results are shown in Fig. E2-41 along with experimental results on several Ladish D6AC steel specimens containing two coplanar semielliptical surface flaws. The curves are plotted in terms of stress-intensity magnification ratio (K_1/K_2) versus flaw spacing ratio (d/a). Probably the most significant point is that there is very little interaction between coplanar flaws unless they are surprisingly close together.

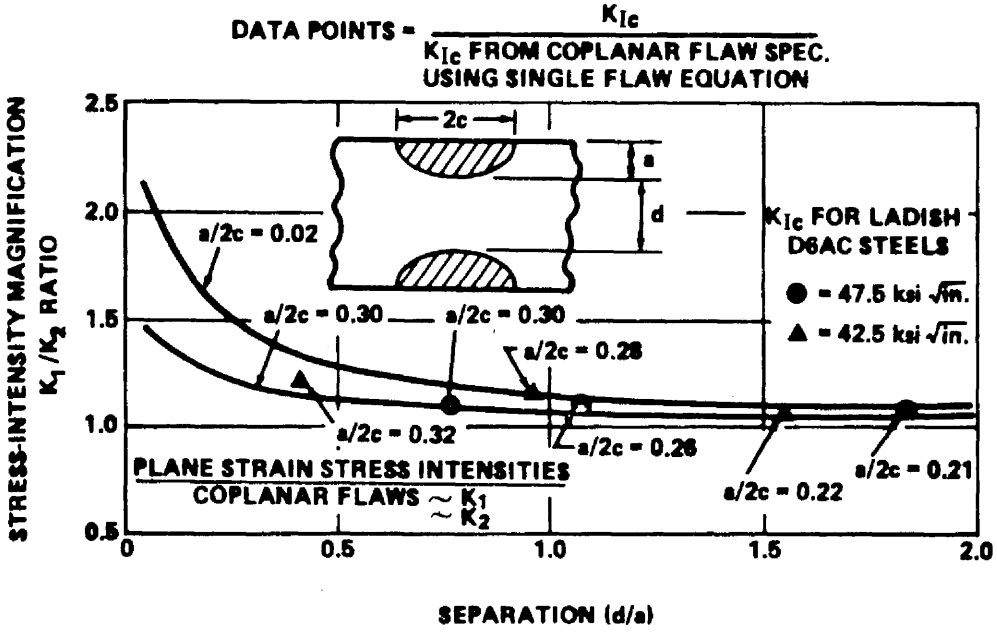

FIGURE E2-41. STRESS-INTENSITY MAGNIFICATION FOR TWO COPLANAR ELLIPTICAL FLAWS

The establishment of NDI acceptance limits when service life requirements are known might best be shown by an illustrative example involving a hypothetical pressure vessel that is expected to encounter a rather complex loading history.

Figure E2-42a shows the assumed service life requirement consisting of one proof-test cycle (at a stress level of α times the operating stress) followed by 1000 cycles and then 100 hr, both at a constant operating stress level of ($\sigma = 1.0$). To define the minimum inspection standards required prior to service, it is necessary to determine the critical flaw size, $(a/Q)_{cr}$, at the end of service (Section 2.4.2) and work backwards, evaluating all portions of the loading profile that can cause flaw growth.

Figure E2-42b represents a dimensionless relationship of stress-to-flaw size as shown previously (Fig. E2-6). The ordinate now is plotted in terms of percentage of critical flaw size at operating stress. Figures E2-42c and d are schematic representations of the cyclic load flaw growth and sustained load flaw growth, respectively.

The approach is as follows:

1. The critical flaw size at operating stress is represented as 100 percent of critical and is the maximum allowed at time T_D (at the end of the service life).

2. Maximum allowed flaw size at time T_C is shown by Point C and represents the maximum allowable flaw size at the start of the 100-hr sustained stress period.

3. The effect of cyclic loading is shown in Fig. E2-42c by moving 1000 cycles from T_C to T_B. Point B then represents the maximum allowable size at time T_B or at the start of the 1000-cycle period. This size is the maximum allowable size before the vessel is placed in service.

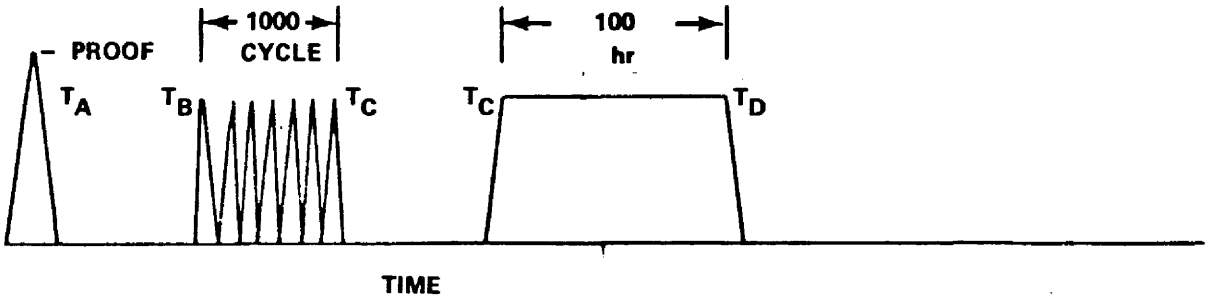

a. Service life requirement.

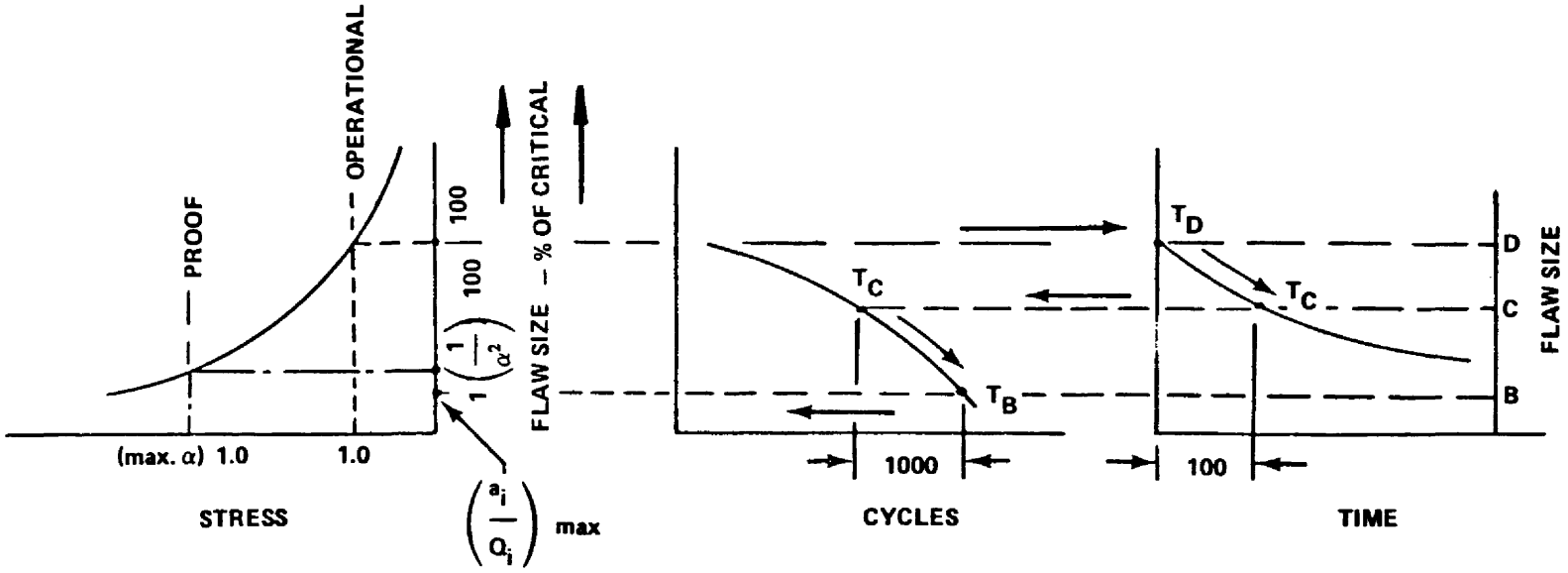

b. c. d.

FIGURE E2-42. DETERMINATION OF NONDESTRUCTIVE INSPECTION ACCEPTANCE LIMITS

4. It can be shown that the previous one-cycle proof test generally has a negligible effect on flaw growth compared with the chosen service life.

Note in this schematic illustration that the maximum allowable flaw size is less than that which could have been present during a successful proof test, and thus the proof test could not guarantee successful fulfillment of the service life requirement. As a result, NDI must be capable of detecting flaws as small as $(a_i/Q_i)_{max}$.

If it is determined that inspection technique limitations preclude the assurance of service life reliability, then either the proof-test factor must be increased to assure that $(a_i/Q_i)_{max}$ is the largest possible existing flaw size at the beginning of service life, or conservative assumptions might be made about flaw geometry and orientation to account for the inability to detect small flaw depths. For example, the length (L) of an indication seen in X-ray inspection could be assumed to be the minor axis of an elliptical flaw where the major axis is large with respect to the minor axis (i.e., $L = 2a$, $Q \approx 1.0$). Consequently, the critical flaw size must be larger (and the operating stress lower) in order to meet the service life requirements. In other words, both $(a_i/Q_i)_{max}$ and $(a/Q)_{cr}$ move higher up the ordinate of Fig. E2-42b.

It should be noted that in terms of "percentage of critical," flaw size is independent of actual stress and toughness values. Obviously, the determination of finite maximum allowable flaw sizes (or smallest flaw size for NDI detection) requires a detailed knowledge of applied stresses in the various tank locations and of the fracture toughness of the materials used. This has been illustrated by the Example Problem A in Section 2.4.3.2 in which the allowable initial flaw size in an aluminum alloy pressure vessel is calculated based on a required service life. In the case where NDI acceptance limits are being considered, the calculated initial flaw depth and length are the minimum demensions which NDI must be capable of detecting.

2.4.3.4 Proof-Test Factor Selection.

It has been previously noted that a successful proof test determines the maximum possible flaw size which can exist after the proof test and prior to the beginning of service. The proof test is the most powerful inspection test presently available and offers the most reliable method for guaranteed service life.

Figure E2-43 shows a schematic theoretical relationship between the critical flaw size, $(a/Q)_{cr}$, and the corresponding fracture stress, as previously illustrated in Fig. E2-6, along with a similar relationship between initial flaw size $(a/Q)_i$ and stress level. The relationships hold true for applied stresses below the yield strength of the material. For stresses above

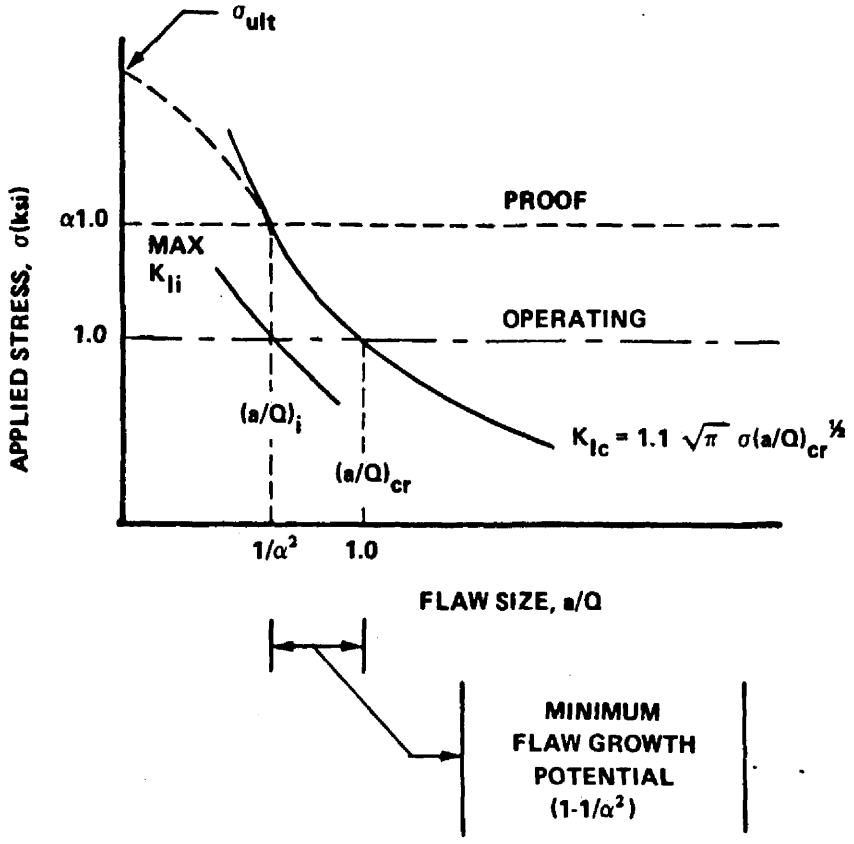

FIGURE E2-43. TYPICAL MATERIAL STRESS-INTENSITY RELATIONSHIP

the yield value the relationships follow some experimentally determined curve up to the ultimate strength, σ_{ult}. If proof pressure is α times the operating pressure, the critical flaw size is

$$(a/Q)_{cr_{proof}} = \max (a/Q)_{i_{oper}} = \frac{1}{1.21\,\pi}\left(\frac{K_{Ic}}{\alpha\,\sigma_{oper}}\right)^2$$

and

$$(a/Q)_{cr_{oper}} = \frac{1}{1.21\,\pi}\left(\frac{K_{Ic}}{\sigma_{oper}}\right)^2 .$$

Thus the proof-test factor, α, is a function of the maximum initial flaw size and critical flaw size for the operating pressure level

$$\frac{(a/Q)_{i_{oper}}}{(a/Q)_{cr_{oper}}} = \frac{1}{\alpha^2} .$$

Since subcritical flaw growth is a function of the initial stress intensity as compared with the critical value, the proof-test factor can be related as

$$\frac{\max K_{Ii}}{K_{Ic}} = \frac{1.1\sqrt{\pi}\,\sigma_{oper}\,(a/Q)^{1/2}_{i_{oper}}}{1.1\sqrt{\pi}\,\alpha\,\sigma_{oper}\,(a/Q)^{1/2}_{i_{oper}}} = \frac{1}{\alpha} ,$$

where K_{Ii} is the initial stress intensity at the operating stress level and temperature, and K_{Ic} is the fracture toughness value at proof test

temperature. It should be noted that lower proof test factors (and therefore lower proof stresses) can be employed if the proof test is performed at a temperature where the material has a lower K_{Ic} than at operating temperature and, consequently, greater susceptibility to flaws. In this way the risk of proof-test failure is minimized insofar as practical.

The maximum K_{Ic} at proof temperature should be employed in the equation rather than the minimum or average K_{Ic} because it results in the selection of a higher proof factor, a conservative event. Figure E2-44 illustrates the difference between the use of maximum and minimum K_{Ic} at proof temperature. For a given maximum initial flaw size, $(a/Q)_i$ (ma), the proof stress required by K_{Ic} (min.) is less than that required by K_{Ic} (max.). In fact, if K_{Ic} (min.) were used and a component fabricated from material characteristic of K_{Ic} (max.) and containing a flaw slightly longer than $(a/Q)_i$ (ma) were proof tested at the lower level, the component would pass

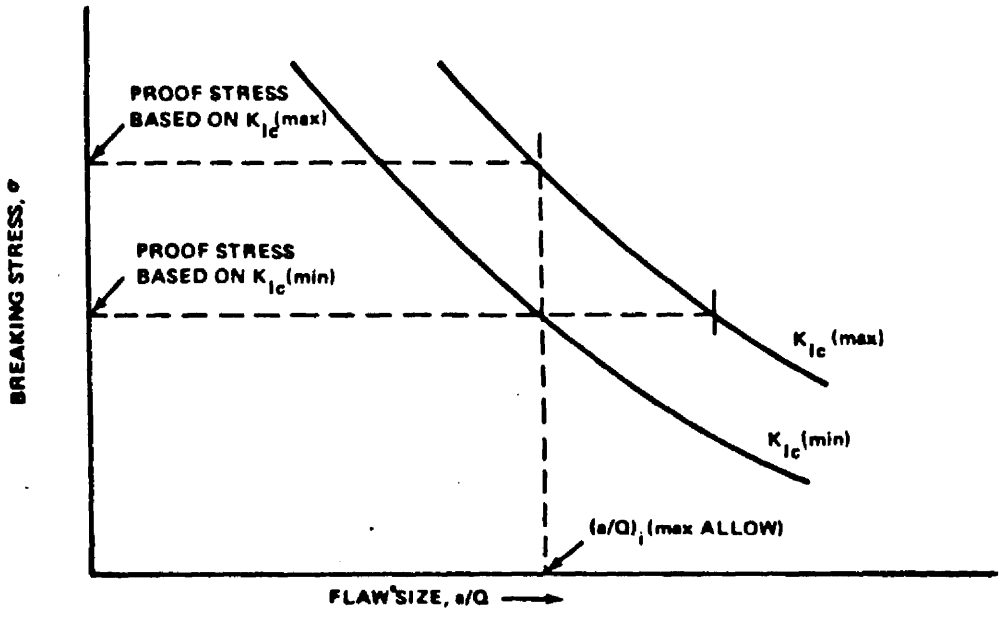

FIGURE E2-44. DETERMINATION OF PROOF STRESS BY MAXIMUM AND MINIMUM VALUES OF K_{Ic}

the proof test successfully but probably would fail in service. The use of $K_{Ic}\ (max)_p$ in the proof-factor equation precludes this.

It has been shown by analysis that regardless of the structural wall thickness, the required minimum proof-test factor α is always $1 \div$ allowable K_{Ii}/K_{Ic}. However, the value of the proof test in providing assurance against service failure changes with decreasing wall thickness and/or increasing fracture toughness, K_{Ic}, the same as occurs with the predicted pressure vessel failure mode. This is discussed in more detail in Ref. 22 and illustrated in Fig. E2-45.

Having experimentally obtained the cyclic and sustained flaw growth for a material under consideration, the necessary proof-test factor can be determined to assure that the structure will meet the service life requirements. Proof-factor determination can be applied to at least two general problem areas in the design of structural components:

1. Evaluation and modification of proof-test conditions for current components for which operating stress and mission are already fixed.

2. Preliminary design of components intended for known missions, including selection of material, maximum operating stress, minimum proof stress, and proof temperature.

The following sample problem illustrates the proper selection of a proof-test factor for a hypothetical pressure vessel design.

I. Example Problem A.

Suppose that a thick-walled liquid nitrogen 5Al-2.5Sn (ELI) titanium pressure vessel must meet a service life requirement of 600 pressure cycles where the pressure is sustained for a prolonged period during each cycle. The vessel has already been successfully proof tested with LN_2 to a proof factor

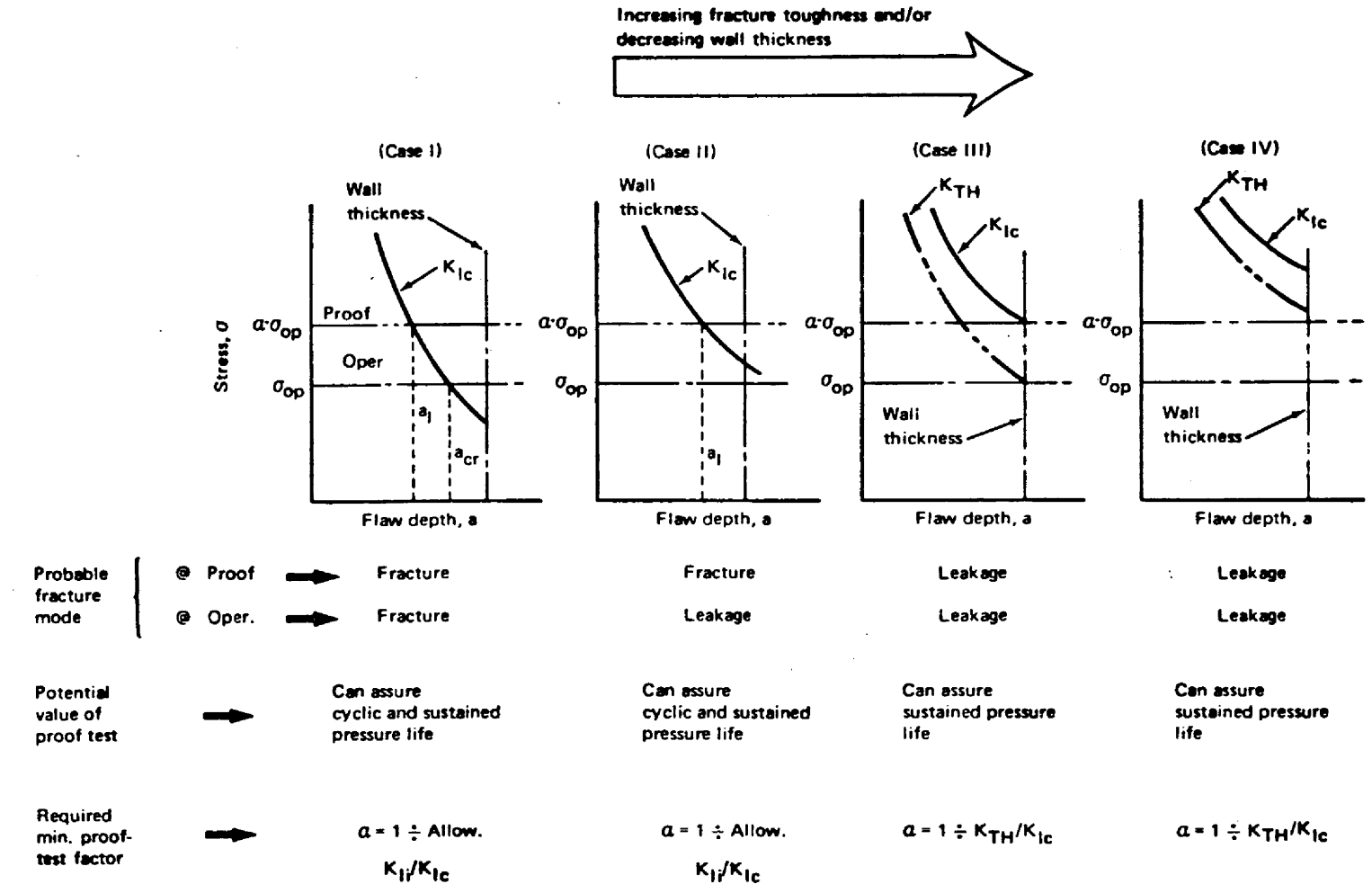

FIGURE E2-45. EFFECT OF WALL THICKNESS ON VALUE OF PROOF TEST

α = 1.25. Will this proof factor assure that no failure occurs during the service life and if not, what proof factor is required?

The cyclic life curve for 5Al-2.5Sn (ELI) titanium is reproduced in Fig. E2-36. The estimated threshold stress-intensity value for sustained-stress flaw growth (K_{TH}/K_{Ic}) is approximately 0.92.

For long hold time, max. $K_{Ii}/K_{Ic} = 1/\alpha = 1/1.25 = 0.80$. From Fig. E2-36 for $K_{Ii}/K_{Ic} = 0.80$, N = 300 cycles. For $K_{TH}/K_{Ic} = 0.92$, N = 100 cycles.

In 300 cycles minus 100 cycles, or 200 cycles, the stress intensity would have reached the estimated threshold value for sustained-stress flaw growth. Thus the predicted minimum life would be only 200 cycles and the proof factor of 1.25 will not assure a service life of 600 cycles.

For 100 cycles plus 600 cycles, or 700 cycles,

$$K_{Ii}/K_{Ic} = 0.70 = \frac{1}{\alpha}$$

and

$$\alpha = \frac{1}{0.70} = 1.43 \quad ,$$

Thus, the 600-cycle service life requires a proof-test factor of 1.43 times the operating pressure.

REFERENCES

1. Fracture Toughness Testing and its Applications. ASTM Special Technical Publication No. 381, American Society for Testing and Materials, April 1965.

2. Irwin, G. R.: Fracture and Fracture Mechanics Report No. 202, T&AM Department of Theoretical and Applied Mechanics, University of Illinois, October 1961.

3. Irwin, G. R.: Crack Extension Force for a Part-Through Crack in a Plate. Journal of Applied Mechanics, Vol. 84 E, No. 4, December 1962.

4. Green, A. E.; and Sneddon, I. N.: The Distribution of Stress in the Neighborhood of a Flat Elliptical Crack in an Elastic Solid. Proceedings of the Cambridge Philosophical Society, Vol. 46, 1959.

5. Kobayashi, A. S.: On the Magnification Factors of Deep Surface Flaws. Structural Development Research Memorandum No. 16, The Boeing Co., December 1965.

6. Plane Strain Crack Toughness Testing. ASTM Special Technical Publication No. 410, American Society for Testing and Materials, December 1967.

7. Review of Developments in Plane Strain Fracture Toughness Testing. ASTM Special Technical Publication No. 463, American Society for Testing and Materials, September 1970.

8. Paris, P. C.; and Erdogan, F.: A Critical Analysis of Crack Propagation Laws. Journal of Basic Engineering, Transactions of the ASME, Series D, Vol. 85, 1963.

9. Foreman, R. G.; Kearney, V. E.; and Engle, R. M.: Numerical Analysis of Crack Propagation in Cyclic-Loaded Structures. Journal of Basic Engineering, Transactions of the ASME, September 1967.

10. Hudson, M. C.: Effect of Stress Ratio on Fatigue-Crack Growth in 7075-T6 and 2024-T3 Aluminum-Alloy Specimens. NASA TN D-5390, August 1969.

REFERENCES (Continued)

11. Tiffany, C. F.; Lorenz, P. M.; and Hall, L. R.: Investigation of Plane-Strain Flaw Growth in Thick-Walled Tanks. NASA CR-54837, 1966.

12. Fracture Control of Metallic Pressure Vessels. NASA SP-8040, May 1970.

13. Wheeler, O. E.: Spectrum Loading and Crack Growth. Transactions of the ASME, Journal of Basic Engineering, March 1972.

14. Elber, W.: Fatigue Crack Closure Under Cyclic Tension. Engineering Fracture Mechanics, Vol. II, No. 1, Pergamon Press, July 1970.

15. Elber, Wolf: The Significance of Fatigue Crack Closure. Damage Tolerance in Aircraft Structures, ASTM Special Technical Publications 486, American Society for Testing and Materials, 1971, pp. 230-242.

16. Pellissier, G. E.: Some Microstructural Aspects of Maraging Steel in Relation to Strength and Toughness. Technical Documentary Report RTD-TDR-63-4048. Air Force Materials Laboratory, Wright-Patterson Air Force Base, Ohio, November 1963.

17. Tiffany, C. F.; and Masters, J. N.: Applied Fracture Mechanics. ASTM Special Technical Publication No. 381, American Society for Testing and Materials, April 1965.

18. Wessel, E. T., et al. Engineering Methods for the Design and Selection of Materials Against Fracture. AD 801005, June 1966.

19. Progress in the Measurement of Fracture Toughness and the Application of Fracture Mechanics to Engineering Problems. American Society for Testing and Materials Special Committee on Fracture Testing of High-Strength Metallic Materials, Materials Research and Standards, Vol. 4, No. 3, March 1964, p. 107.

20. Pyle, R.; Schillinger, D. E.; and Carman, C. M.: Plane Strain Fracture Toughness and Mechanical Properties of 2219-T87 Aluminum and 5AL-2.5Sn(ELI) Titanium Alloy Weldments and One Inch Thick 5AL-2.5Sn(ELI) Titanium Alloy Plate. NASA CR-72154, Department of the Army, Frankfort Arsenal, September 1968.

REFERENCES (Concluded)

21. Wilhem, D. P.: Fracture Mechanics Guidelines for Aircraft Structural Applications. AFFDL-TR-69-111, Northrop Corp., February 1970.

22. Shah, R. C.: Fracture Mechanics Assessment of Apollo Launch Vehicle and Spacecraft Pressure Vessels. Vol. 1, Report D2-114248-1, The Boeing Co., November 1968.

23. Kobayashi, A. S.; and Hall, L. R.: On the Correction of Stress Intensity Factors for Two Embedded Cracks. Structural Development Research Memorandum No. 9, The Boeing Co., 1963.